Identifying the reactivity of photochemically produced reactive intermediates with dissolved organic matter

by

Edward G. Kostelnik

A thesis submitted in partial fulfillment of

the requirements for the degree of

Master of Science

(Environmental Chemistry and Technology)

at the

UNIVERSITY OF WISCONSIN-MADISON

2024

Abstract

Photolysis of dissolved organic matter (DOM) is a critical pathway in the carbon cycle of inland lakes. Complete photooxidation releases carbon dioxide (CO_2), while partial photooxidation results in the incorporation of oxygen (O_2) into DOM and subsequent transformation of DOM. Both complete and partial photooxidation can be highly influenced by indirect photolysis, which occurs when photochemically produced reactive intermediates (PPRI) transform DOM. However, which PPRI and reaction mechanisms are most important to DOM photooxidation remains unclear. In this study, DOM was collected from 11 inland lakes of differing trophic status to investigate the role of PPRI in complete and partial photooxidation of DOM. Quencher studies of singlet oxygen ($^1O_2$), hydroxyl radical ($^\bullet$OH), and triplet DOM (^{3}DOM), along with Fourier transform-ion cyclotron resonance mass spectrometry (FT-ICR MS) analysis, were used to identify the roles of these PPRI in the partial and complete photooxidation of DOM. Consequently, all PPRI investigated were found to play a role in complete and partial photooxidation in a diverse set of DOM. For example, $^1O_2$ contributed to the oxidation of DOM, $^\bullet$OH participated in oxidation and complete photooxidation in some samples, and ^{3}DOM played a role in complete photooxidation. Overall, these results give insight into how DOM reactivity influences CO_2 production in inland lakes.

To my family and the love of my life Grace Fleszewski

I could not have done this without the support and love from you all.

Acknowledgments

I would like to take the time to sincerely thank the people around me who made this possible. First, I would like to thank my thesis advisor Christy Remucal for all your help and support throughout the process. I would also like to thank my thesis committee Dr. Christy Remucal, Dr. Matt Ginder Vogel, and Dr. Haoran Wei for your support, time, and effort in the process. Additionally, I would like to thank the staff at WSEL including James Lazarcik, M.S., and Sara Haney for their continued support and help with the research I was able to conduct at the University of Wisconsin-Madison.

Next, I would also like to thank my family and friends for their continued support throughout the entire process. My mom, Jennifer Kostelnik, brothers Danny and Joe Kostelnik and sister Anna Kostelnik have helped make me who I am today, and I would not be here without them. My friends Tom Paul and Noah Moriarty have supported me throughout the entire process, I could not have done it without you all either. I love you all so much and I am so blessed to be able to share more experiences in life and be there to support you all through thick and thin in the same way you all did for me.

Lastly, I would like to thank my partner, Grace Fleszewski. Your love and support never go unnoticed and are so unconditional and true. I am so honored to be able to be with you, to share life with you. You have changed my life for the better and I cannot imagine a life without you. Thank you for always being there, for always loving me, for always supporting me. This journey would not have been the same without you. I love you, Grace. I cannot express how excited I am to spend the rest of my days being able to identify plants at bogs and birds on the Great Lakes with you. To our next adventure together, Michigan.

Table of Contents

List of Figures

≥10%. Each individual graph represents a treatment from Fish Lake (E2) including (a) -•OH (IPA), (b) -$^1O_2$ (FFA), (c) -^{3}DOM (SA), and (d) All PPRI.

Figure S8: Relative formula intensity increase/decrease van Krevelen diagrams, with blue representing formula intensity decreases ≥10% and red representing formula intensity increases ≥10%. Each individual graph represents a treatment from Big Muskellunge Lake (O1) including (a) -•OH (IPA), (b) -$^1O_2$ (FFA), (c) -^{3}DOM (SA), and (d) All PPRI.

Figure S9: Bar graphs demonstrating the number of oxygen additions and carbon dioxide loss in each sample water and treatment. Red represents one oxygen addition, blue represents two oxygen additions, green represents either one or two oxygen additions, and purple represents carbon dioxide loss. Each individual graph represents a sample water including (a) D1, (b) D2, (c) M1, (d) E1, (e) E2, and (f) O1.

Figure S10: van Krevelen diagrams demonstrating the DOM compositional differences in oxygen addition and carbon dioxide loss in each sample water and treatment. Red represents carbon dioxide loss formulas and blue represents total oxygen addition formulas. Each individual graph represents a treatment from Trout Bog (D1) including (a) -•OH (IPA), (b) -$^1O_2$ (FFA), (c) -^{3}DOM (SA), and (d) All PPRI.

Figure S11: van Krevelen diagrams demonstrating the DOM compositional differences in oxygen addition and carbon dioxide loss in each sample water and treatment. Red represents carbon dioxide loss formulas and blue represents total oxygen addition formulas. Each individual graph represents a treatment from Crystal Bog (D2) including (a) -•OH (IPA), (b) -$^1O_2$ (FFA), (c) -^{3}DOM (SA), and (d) All PPRI.

Figure S12: van Krevelen diagrams demonstrating the DOM compositional differences in oxygen addition and carbon dioxide loss in each sample water and treatment. Red represents carbon dioxide loss formulas and blue represents total oxygen addition formulas. Each individual graph represents a treatment from Allequash Lake (M1) including (a) -•OH (IPA), (b) -$^1O_2$ (FFA), (c) -^{3}DOM (SA), and (d) All PPRI.

Figure S13: van Krevelen diagrams demonstrating the DOM compositional differences in oxygen addition and carbon dioxide loss in each sample water and treatment. Red represents carbon dioxide loss formulas and blue represents total oxygen addition formulas. Each individual graph represents a treatment from Lake Monona (E1) including (a) -•OH (IPA), (b) -$^1O_2$ (FFA), (c) -^{3}DOM (SA), and (d) All PPRI.

Figure S14: van Krevelen diagrams demonstrating the DOM compositional differences in oxygen addition and carbon dioxide loss in each sample water and treatment. Red represents carbon dioxide loss formulas and blue represents total oxygen addition formulas. Each individual graph represents a treatment from Fish Lake (E2) including (a) -•OH (IPA), (b) -$^1O_2$ (FFA), (c) -^{3}DOM (SA), and (d) All PPRI.

List of Tables

Chapter 1. Identifying the reactivity of photochemically produced reactive intermediates with dissolved organic matter

Prologue: Chapter 1 was a collaboration between Edward Kostelnik and Christy Remucal. This is a draft manuscript that will be submitted for publication. EK analyzed samples and wrote the manuscript while CR was the principal investigator.

Introduction

Understanding global carbon cycling is increasingly important in the face of increasing effects of climate change. Within the global carbon cycle, inland surface waters, like lakes, play an important role in the storage, transport, and processing of organic carbon.[1,2] One example of the processing of organic carbon in lakes is through the mineralization of dissolved organic matter (DOM). This process can result in the release of carbon dioxide (CO_2) into the atmosphere. Inland surface waters are responsible for carbon emissions around 2 Pg-C/yr, which is around 5.7% of the carbon emissions from anthropogenic sources in 2021 (34.9 Pg-C/yr).[3,4] Consequently, DOM processing in inland surface waters is important to consider in terms of global carbon cycling and emissions.[5]

Dissolved organic matter (DOM) is a complex mixture of organic molecules that are derived from microbial or terrestrial sources. DOM can undergo both biological and photochemical transformations in aquatic systems. Biological transformation through microbial processing of DOM has large impacts on DOM composition and reactivity and is widely considered to be the major driver of DOM transformation in lakes.[6–8] For example, studies have shown up to 60% of DOM degradation results from microbial processing.[9,10] However, both biological and photochemical processes can result in large impacts on DOM transformation or

mineralization (i.e., release of CO_2) depending on environmental conditions and initial DOM composition. Recent studies suggest photochemical transformations may play a more important role in both DOM transformations and mineralization than previously thought. For example, up to 33% of CO_2 production in Artic rivers has been attributed to photochemical transformation.[11] Changes in DOM composition from photochemical transformations has consequences for its subsequent reactivity. Previous studies have indicated that DOM becomes less aromatic and decreases in molecular weight after photochemical transformation.[7,12–18] Additionally, studies using high-resolution mass spectrometry demonstrated that oxidation in DOM samples can increase or decrease even if generally they are showing a trend toward more saturated photoproducts.[6,15,19–24] Overall, these results indicate that photochemical transformation pathways are not negligible and should be considered in the global carbon cycle.

DOM is known to undergo either direct photochemical transformation or indirect photochemical transformations. In direct photochemical transformation, sunlight interacts with DOM directly and results in its transformation. Indirect photochemical transformation is characterized by sunlight interacting with DOM and producing photochemically produced reactive intermediates (PPRI), such as singlet oxygen ($^1O_2$), hydroxyl radical ($^{\bullet}OH$), and triplet DOM (^3DOM), which then interact with DOM to result in its transformation.[25–29] The resulting DOM transformations are labelled as partial or complete photooxidation. Complete photooxidation signifies the production of CO_2 (i.e., complete mineralization) and partial photooxidation signifies the incorporation of oxygen into DOM. In some studies, the presence of PPRI have been shown to affect the partial and complete photooxidation of DOM. For example, $^1O_2$ has been shown to react with DOM quickly and be involved in partial photooxidation.[6,27,30,31] Additionally, $^{\bullet}OH$ has been shown it can be responsible for around 4% of complete photooxidation, although partial

photooxidation was not investigated.[32,33] ^{3}DOM has not been investigated in this manner at all. In general, the roles of specific PPRI in DOM transformation and how DOM composition effects its susceptibility to these transformations has not been well studied.

Overall, it is not well known how PPRI influence DOM transformation and how these transformations contribute to the global carbon cycle. To address this knowledge gap, this study set out to investigate the responsibilities of each PPRI in the transformation of DOM. To do this, photolysis experiments were conducted with DOM that ranged widely in composition in the presence and absence of quenchers. These quenchers were able to help suppress specific PPRI from the sample and allow for in depth analysis of DOM transformational changes before and after photolysis using high-resolution mass spectrometry. We hypothesized that singlet oxygen was the main driver in partial photooxidation of DOM throughout the study, with hydroxyl radicals and triplet DOM being more minorly involved in both complete and partial photooxidation.

Methods

Materials. All materials were used as received (**Supporting Information Section S1**). Ultrapure water (18.2 MΩ cm) was obtained from a Milli-Q water purification system.

Sample collection. Samples were collected from the North Temperate Lakes-Long Term Ecological Research (NTL-LTER) network encompassing inland lakes in northern and south-central Wisconsin shown in **Table S1**. Northern lakes included Trout Lake, Trout Bog, Crystal Lake, Crystal Bog, Allequash Lake, Sparkling Lake, and Big Muskellunge Lake. Southern lakes included Lake Mendota, Lake Monona, Fish Lake, and Lake Wingra. Near surface samples were collected in 4 L amber glass bottles near buoys located in the middle of the lakes in November

2022 (**Table S1**). Each sample was filtered using a 0.45 μm glass fiber filter within a week of sample collection. Samples were stored in clean 4 L amber jugs in the dark at 4 °C (**Section S2**).

Bulk water chemistry. Dissolved organic carbon (DOC) and dissolved inorganic carbon (DIC) were measured using a Shimadzu Total Organic Carbon analyzer. Anions including sulfate, nitrate, and chloride were measured by ion chromatography. Cation concentrations were taken from the NTL-LTER data release around the sampling time.[34] pH was measured using a Mettler Toledo EL20 pH meter. Additional details regarding these measurements can be found in **Section S3**.

General bulk DOM composition was measured using UV-visible (UV-vis) and fluorescence spectroscopy. UV-vis spectra were collected using a Shimadzu 2401PC Recording Spectrophotometer. The analysis was done in triplicate using 1 nm increments in the range of 200-800 nm. Specific UV absorbance ($SUVA_{254}$) was calculated as the absorbance at 254 nm divided by the DOC concentration in each sample.[35] E_2:E_3 was calculated using a ratio of absorbance at 250 nm to 365 nm.[36] Fluorescence excitation-emission matrices were collected using a Horiba Aqualog Fluorimeter in 4 nm increments in the range of 250-800 nm. Indices including the fluorescence index (FI) and biological index (BIX) were calculated as described in (**Table S4**).[37–39] Further details can be found in **Section S3**.

General photochemical reactivity. Steady-state concentrations and quantum yields or quantum yield coefficients for ^{3}DOM were quantified for PPRI including $^1O_2$, $^{\bullet}$OH, and ^{3}DOM throughout sampled lakes. Samples were amended with probe compounds and irradiated in a Rayonet photoreactor equipped with 365 nm bulbs (full width half max = ±10), which is within the solar spectrum.[40] Previous studies have investigated nitrate photolysis and found it to be negligible under these irradiation conditions.[23] Probe compounds consisted of furfuryl alcohol

(FFA), terephthalic acid (TPA), and 2,4,6-triemthylphenol (TMP) all at 10 μM. Irradiations were performed in triplicate for each water and run alongside a triplicate of an actinometer (*p*-nitroanisole and pyridine) to quantify light intensity.[41,42] Degradation of TMP and FFA and formation of hydroxyterephthalic acid (hTPA) were measured by high-performance liquid chromatography (HPLC).[23,43] More information on these methods can be found in **Section S4**.

Quenching experiments. Quenching experiments were conducted on a subset of lakes including two dystrophic lakes, one mesotrophic lake, two eutrophic lakes, and one oligotrophic lake (**Section S5**). Each of these lakes had varying PPRI concentrations and were chosen to include diverse sets of DOM composition and PPRI concentrations. Experiments using quenching molecules were done to eliminate specific PPRI and analyze the change in DOM composition when the specific PPRI was eliminated compared against unquenched controls. Thus, diverse DOM composition and PPRI concentrations in each of these lakes provided a wide variety of changes that could be linked to specific PPRI.

To accomplish these quenching experiments, 24-hour irradiations using a Rayonet photoreactor was done in 250 mL borosilicate glass bottles.[24] This volume was used to accommodate solid phase extraction (SPE) before FT-ICR MS analysis. Quenchers consisted of furfuryl alcohol (FFA), isopropyl alcohol (IPA), and sorbic acid (SA). Quencher concentrations ranged from 100 μM for SA (due to solubility issues) to 10 mM in FFA and IPA. Quenchers were used to suppress the activity of specific PPRI: FFA suppressed $^1O_2$, IPA suppressed $^{\bullet}OH$, and SA suppressed ^{3}DOM. 2,4,6-Trimethylphenol (TMP) was tested as an alternate ^{3}DOM quencher and issues with an increase in nitrogen formula matching suggested another quencher like sorbic acid (SA) may better suited for the analysis (**Section S6**). Experimental set up consisted of each lake being split into a total of 8 samples: 4 samples that went through photolysis and 4 samples that

were dark controls. Of the irradiated samples, one was quenched with FFA, one was quenched with IPA, one was quenched with SA, and one was unquenched. The nonirradiated samples followed the same setup. When compared to the irradiated sample, the nonirradiated dark controls helped track changes due to the quencher itself. The irradiated samples, after accounting for dark control changes, were then compared to the unquenched irradiated sample to analyze PPRI responsibility.

After the 24-hr experimental period, DOM was extracted from the samples using solid phase extraction (SPE).[44–46] Samples (250 mL) were acidified using 1M HCl to pH ~2.0 and loaded onto BondElut PPL cartridges. Samples were run through the cartridges and extracted using 5 mL of methanol. The sample extracts were then stored at 4ºC until high-resolution mass spectrometry was performed. Further details on these methods are found in **Section S6**.

High-resolution mass spectrometry. Molecular composition of DOM was analyzed using a Bruker SolariX XR 12T Fourier transform-ion cyclotron mass spectrometer (FT-ICR MS). SPE sample extracts were diluted 20x in 60:40 acetonitrile: water and directly injected into the FT-ICR MS using negative mode electrospray ionization (voltage = -1.4 kV; gas pressure = 0.3 psi; 350 readings per sample). Accumulation times were kept constant at 0.1 s and the total ion chromatograph intensity was constant in each scan. Ions were only exported if they contained a signal-to-noise ratio >3. The exported *m/z* ions were linearly calibrated using known DOM formulas described previously.[42,47,48] After calibration the DOM formulas were compared to potential formulas with combinations of $C_{0\text{-}80}{}^{13}C_{0\text{-}1}H_{0\text{-}140}N_{0\text{-}2}S_{0\text{-}1}$. Formulas were then matched if they were part of a homologous series (+CH2 or CH4 vs. O) with three members and had a formula mass error <0.5 ppm.[49] After matching, weighted averages of hydrogen to carbon ($H:C_w$), oxygen to carbon ($O:C_w$), and double bond equivalents (DBE_w) were calculated.[47] Further analysis

between the controls with no quenchers and the 24 hour irradiated samples was done including changes in relative formula intensity (≥ 10% change) and loss of CO_2 formulas and addition of O formulas which are further detailed in **Section S6**.

Results and Discussion

Bulk DOM characteristics. Bulk DOM characteristics show a wide range of initial DOM composition. Eutrophic (E1 and E2) and oligotrophic (O1) lakes in the study are characterized by DOM that is more aliphatic (low $SUVA_{254}$), lower in apparent molecular weight (high E_2:E_3), and reduced (low O:C_w; **Table S5**). The samples taken in these lakes correspond to more processed and/or microbially-derived DOM (high FI; high BIX).[38,50] In contrast, dystrophic (D1 and D2) and mesotrophic (M1) lakes sampled in the study are characterized by more aromatic (high $SUVA_{254}$), higher apparent molecular weight (lower E_2:E_3), and oxidized (high O:C_w) DOM (**Table S5**). The samples taken in these lakes correspond to more terrestrially-derived DOM (low FI; low BIX).[50–55]

DOM compositional changes post-photolysis. DOM in select sample waters demonstrated a shift towards less aromaticity (decrease in $SUVA_{254}$) after photolysis (**Table S11**; **Figure S2**). While the changes in metrics derived from UV-vis spectra are consistent with a shift towards more processed DOM, variability was observed in indices derived from fluorescence spectra. BIX increased in all samples after photolysis, which is consistent with more processed DOM. In contrast, the consistent decreases in FI indicated DOM was becoming more terrestrial (i.e., less processed). The contradictory FI results agreed with a previous study stating photooxidation could result in complexities that make fluorescence indices hard to use to assign DOM origins.[24]

Molecular levels changes in DOM composition were also analyzed to investigate more specific changes in DOM composition after photolysis. DOM transformation was variable when comparing $H:C_w$ and $O:C_w$ ratios (**Figure 1**). For example, decreased $H:C_w$ and increased $O:C_w$ was seen in samples D1, E1, and O1 (**Table S14**), indicating that the DOM was becoming more aromatic and more oxidized. Additionally, smaller changes in $H:C_w$ or $O:C_w$ were seen in sample waters D2, M1, or E2 (**Table S14**). This variability agrees with a previous study that also found variability in DOM compositional changes post-photolysis.[24] However, other studies have shown DOM composition changes towards more oxidized and aliphatic post-photolysis.[6,7,13,15,19–22,56] Overall, the samples included in this study showed high levels of variation.

Further analysis was done comparing relative intensity changes of assigned formulas before and after photolysis (**Figures S3-S8**). In this analysis, sample waters D1, E1, and O1 showed relative intensity increases in the more oxidized and aromatic formulas post-photolysis. Sample waters D2, E2, and M1 generally showed relative intensity decreases in the more oxidized and aromatic formulas. This further demonstrated the variability between samples, despite similarities in initial DOM composition origin. For example, in sample waters D1 and D2, both dystrophic lakes, the samples are showing opposite trends between each other post-photolysis.

Lastly, analysis was done on the partial and complete photooxidation of DOM in the sample waters. Partial photooxidation was analyzed by matching formulas attributed to the addition of oxygen atoms found in sample waters. This analysis included the addition of a single oxygen atom, two oxygen atoms, and either one or two oxygen atoms. Overall, the lakes ranged from 182 unique oxygen addition formulas in lake O1 to 422 unique oxygen addition formulas in lake D2 (**Figures 3** and **S9**). This suggests that with all PPRI present, the samples showed a wide range of oxygen addition that could be attributed to differences in initial DOM composition. For example, more

terrestrial and aromatic DOM in D2 showed the highest oxygen addition formulas, while the more microbial and aliphatic DOM in O1 showed the lowest oxygen addition formulas (**Figures S10-S15**). Some studies have shown more aromatic DOM is most susceptible to photooxidation, while aliphatic DOM transitions to more reduced DOM.[24,57]

Complete photooxidation was analyzed by matching formulas attributed to the loss of carbon dioxide in sample waters. The lakes ranged from 130 unique carbon dioxide loss formulas in D1 to 480 carbon dioxide loss formulas in E1. This shows that the sample waters analyzed exhibit a wide range of carbon dioxide loss that could be dependent on initial DOM composition like partial photooxidation. For example, more terrestrial and aromatic DOM results in less carbon dioxide loss while more processed and microbial DOM results in more carbon dioxide loss (**Figures 3** and **S9-S15**). More saturated and aliphatic DOM has been connected to decarboxylation processes and could signify a role for decarboxylation in these samples.[24,58]

The role of hydroxyl radical in DOM compositional changes. Hydroxyl radicals contributed to changes in DOM composition, especially in sample waters D1 and E1. Post-photolysis, a transition to more reduced and aliphatic DOM (increase in $H:C_w$; decrease in $O:C_w$) was observed in sample waters D1, D2, M1, and E1 when hydroxyl radicals were quenched with TPA (**Figure 1**). Opposite trends between the unquenched sample with all PPRI and sample waters D1, D2, M1, and E1 without hydroxyl radicals were observed. The opposite trend observed in these sample waters demonstrates that hydroxy radicals were involved in the DOM transformation when analyzing weighted averages derived from FT-ICR MS data. The formation of aliphatic and reduced formulas in the absence of hydroxyl radicals agreed with a previous study that found hydroxyl radicals reacted with more aliphatic and saturated formulas.[58]

Formula intensity changes were determined as either increasing or decreasing from the dark control sample to the irradiated sample. Aliphatic and reduced formulas decreased to the same extent as the unquenched sample in sample waters D2, M1, E2, and O1 (**Figures S3-S8**). This suggests that hydroxyl radicals may not play an important role in these lakes. Additionally, these trends were different then what was suggested with the $H:C_w$ and $O:C_w$ ratios above showing bulk DOM data needs to be interpreted carefully.

However, more reduced and aliphatic formulas were observed in sample water D1 and E1 without hydroxyl radicals when compared to the unquenched sample (**Figures 2**, **S3**, and **S6**). The presence of these opposite trends demonstrates hydroxyl radicals play an important an important role in DOM transformation in these sample waters. These results suggest that hydroxyl radicals may play a role in the formation of more oxidized and aromatic formulas when present in these sample waters. Some studies showed the importance of hydroxyl radicals to processes like hydroxylation and decarboxylation.[59,60] These studies show a possible avenue hydroxyl contribute to an increase in oxidized and aromatic formulas in the sample waters observed here.

The extent of partial photooxidation, as measured by the formation of photoproducts attributable to oxygen addition, was lower in sample waters D1, D2, and E1 compared to the unquenched samples (**Figures 3** and **S9-15**). In the absence of hydroxyl radicals, sample waters showed a range of 180 unique oxygen addition formulas in O1 to 289 unique oxygen addition formulas in E2. Large decreases in oxygen addition formulas were seen in sample waters D1, D2, and E1 when hydroxyl radicals were quenched. These changes showed larger trends when compared to the unquenched sample. This signifies hydroxyl radical has an impact on partial photooxidation in these sample waters. These results also align with the studies discussed above stating hydroxyl radicals have a role in hydroxylation of DOM.[59,60]

Complete photooxidation was different in sample waters D1, O1, and E1 when compared to the unquenched samples (**Figures 3** and **S9-S15**). Sample waters showed a range of 105 unique carbon dioxide loss formulas in E2 to 299 unique carbon dioxide formulas in D1. Decreases in carbon dioxide loss formulas were seen in sample waters E1 and O1, while increases in carbon dioxide loss was seen in sample water D1 when hydroxyl radicals were absent. This shows variation in how hydroxyl radicals are utilized depending on DOM composition. This observation of D1 seems to disagree with previous studies that report decarboxylation as a major pathway for hydroxyl radical DOM transformation.[59,60] However, observations of E1 and O1 agree with this major pathway since carbon dioxide loss decreases when hydroxyl radicals were absent. Overall, the differences between samples waters with hydroxyl radicals absent versus ones with all PPRI present show that hydroxyl radicals can be important depending on initial DOM composition.

The role of singlet oxygen in DOM compositional changes. Singlet oxygen contributed to changes in DOM composition throughout most sample waters analyzed. However, the extent of the changes attributed to singlet oxygen should be carefully considered since this quencher can also react with other PPRI such as hydroxyl radicals.

Post-photolysis, a transition to more oxidized and aromatic DOM (decrease in $H:C_w$; increase in $O:C_w$) in the absence of singlet oxygen when compared to the unquenched sample was seen in all sample waters except D1 (**Figure 1**). In all waters except D1, this transition could signify that singlet oxygen has a role in the transformation of DOM towards more aliphatic and reduced formulas, which seems contradictory given the role of $^1O_2$ as an oxidant. This data does not agree with bulk DOM data from other studies that show a transition to more oxidized and aromatic DOM in the presence of singlet oxygen.[30,61]

Relative intensity changes showed most samples waters transitioning to more oxidized and aromatic formulas in the absence of singlet oxygen except sample waters D1 and D2 (**Figure S3-S8**). This means, when singlet oxygen is present it would be transitioning into more aliphatic and reduced DOM. Decreases in aliphatic and reduced formulas when compared to the unquenched samples were seen in sample waters E1, E2, M1 (**Figure S3-S8**) in the absence of singlet oxygen. In E2, for example, these decreases were moderately different from unquenched samples and are shown in **Figures 2c** and **2d**. In sample waters D1 and D2 general decreases were seen throughout different types of DOM that were relatively similar to the accompanying unquenched sample with all PPRI present. These waters do not follow the trend towards decreases in aliphatic and reduced formulas when singlet oxygen was absent like the other sample waters analyzed. This could signify that singlet oxygen may play a general role in the production of diverse photoproduced formulas in these sample waters.

Analysis was done on the partial and complete photooxidation of samples waters in the absence of singlet oxygen and how that compared to the sample waters with all PPRI present (**Figure S9-S15**). In the absence of singlet oxygen, sample waters ranged from 296 unique oxygen addition formulas in M1 and 539 unique oxygen addition formulas in D1 as seen in **Figure 3b**. In terms of partial photooxidation, sample waters D1, E1, E2, and O1 all showed increases in oxygen addition formulas when singlet oxygen was absent when compared to accompanying unquenched sample with all PPRI present (**Figure 3b**). This could suggest that singlet oxygen may not play a role in partial photooxidation in a diverse set of DOM. This is contradictory to what some studies state, where singlet oxygen is an important oxidant for DOM.[61,62]

Further, in the absence of singlet oxygen, sample waters ranged from 36 unique carbon dioxide loss formulas in M1 to 662 unique carbon dioxide loss formulas in E1 (**Figure 3e**). Sample

waters D1 and E1 showed increases in carbon dioxide loss formulas when singlet oxygen was absent (**Figure 3e**). The other sample waters all showed large scale decreases in carbon dioxide loss formulas when singlet oxygen was absent (**Figure 3e**). This could signify the role of singlet oxygen in complete photooxidation of DOM which does not completely agree with a previous study that shows singlet oxygen as an important component of DOM partial photooxidation.[61] However, there is variation depending on DOM composition, where some sample waters show increases in carbon dioxide loss formulas when singlet oxygen is absent.

The role of triplet DOM in DOM compositional changes. Triplet DOM contributed to a variety of changes in DOM composition throughout sample waters analyzed. However, triplet DOM is known to have a role in the production of other PPRI such as singlet oxygen and hydroxyl radicals and quenching triplet DOM may also decrease the concentrations of other PPRI.[63]

Sample waters M1, E1, and O1 generally develop more oxidized and aromatic DOM in the absence of triplet DOM with some contradiction seen in the $H:C_w$ and $O:C_w$ parameters (**Figure 1**). Sample waters D1 and D2 generally saw more reduced and aliphatic formulas in the absence of triplet DOM. These results generally demonstrate that more terrestrial DOM transitions to more oxidized and aromatic formulas in the presence of triplet DOM, while more microbial DOM does the opposite.

Relative intensity changes showed more terrestrial DOM transition to more reduced and aliphatic in the absence of triplet DOM. In this analysis, sample waters D1 and D2 showed increases in more reduced and aliphatic DOM in absence of triplet DOM compared to the sample containing all PPRI (**Figure S3-S8**). The other lakes generally showed an increase in more aromatic and oxidized DOM, for example, sample water M1 seen in **Figures 2e** and **2f**. In this example, more aromatic and oxidized DOM increased in intensity and more reduced and aliphatic

DOM decreased in intensity when triplet DOM was absent. Overall, depending on DOM composition, triplet DOM could be involved in the oxidation or reduction of DOM. The results of the more microbial lakes tend to agree with studies stating the importance of triplet DOM as a reductant.[64,65] However, more terrestrial based lakes like D1 and D2 demonstrated oxidation which lined up with other studies demonstrating triplet DOM oxidation.[66–69] This variability is characteristic of triplet DOM which is relatively complex. The quencher used in this study, sorbic acid, primarily quenches high energy triplet DOM and leaves other types of triplet DOM available to react.[63] This could contribute to some of the variability seen in these results.

To get into this further, analysis was done on the complete and partial photooxidation of sample waters in the absence of triplet DOM and how that compared to sample waters with all PPRI present (**Figure S9-S15**). In the absence of triplet DOM sample waters ranged from 241 unique oxygen addition formulas in D1 to 389 unique oxygen addition formulas in M1. In terms of partial photooxidation, sample waters D1 and D2 showed a decrease in oxygen addition in the absence of triplet DOM compared to the accompanying sample with all PPRI present (**Figure 3c**). Other sample waters, M1, E1, E2, and O1, all showed increases in oxygen addition in the absence of triplet DOM (**Figure 3c**). These results suggest more terrestrial DOM tends to be more likely to undergo partial photooxidation with triplet DOM present than more microbial sources. One explanation for the differences seen in D1 and D2 so far could be due to the highly aromatic nature of the DOM and its susceptibility of this DOM to direct photolysis.[7,61] Since quenching triplet DOM could potentially slow formation of singlet oxygen and hydroxyl radicals and effectively turn off indirect photolysis, the samples more susceptible to direct photolysis would be hypothesized to show the most change. [63]

Further, in the absence of triplet DOM, sample water ranged from 139 unique carbon dioxide loss formulas in D1 to 197 unique carbon dioxide loss formulas in E1. In terms of complete photooxidation, sample waters D1, D2, E2, and M1 all showed similar carbon dioxide loss formulas when compared to accompanying sample containing all PPRI. This signifies that triplet DOM may not have had a significant effect on complete photooxidation in these waters. However, in sample waters E1 and O1, the absence of triplet DOM significantly reduced the number of carbon dioxide loss formulas compared to the sample with all PPRI present. This could signify triplet DOM responsibility in the complete photooxidation of these lakes.

Environmental Implications

Overall, this study was able to find evidence for roles of all three investigated PPRI in the transformation of DOM throughout diverse sample waters. First, hydroxyl radicals played an important role in the partial and complete photooxidation of some dystrophic and eutrophic lakes in this study (**Figures 2**, **3**, and **S9-S15**). They also contributed to the transition of DOM towards more aromatic and oxidized in these lakes (**Figures 1** and **S3-S8**). However, most lakes did not show a large change when hydroxyl radicals were quenched.

Second, singlet oxygen played a small part in DOM oxidation. However, it was seen to have an important role in complete photooxidation. This result should be interpreted carefully because the quencher chosen for singlet oxygen can also quench hydroxyl radicals unselectively. However, singlet oxygen generally contributed to more aliphatic and reduced DOM in most lakes analyzed (**Figures 1** and **S3-S8**). It also contributed to increases in complete photooxidation and the release of carbon dioxide in most lakes analyzed (**Figures 2**, **3**, and **S9-S15**).

Lastly, triplet DOM played an important role in the partial photooxidation of these lakes and a less role in the complete photooxidation in these lakes. However, these results should also

be considered carefully because quenching triplet DOM effectively also quenches hydroxyl radical and singlet oxygen production. Regardless, the quenching of triplet DOM demonstrated increased oxidation/partial photooxidation in more terrestrial sourced DOM in comparison to reduction of more microbial DOM (**Figures 2,3; S9-S15**). This could be caused by the increased likelihood for terrestrial DOM to undergo direct photolysis, which is effectively produced here since the quenching of triplet DOM also inhibit some of the singlet oxygen and hydroxyl radical production.

Future work

Two important future ideas to consider involve furthering the knowledge of how PPRI influences specific reaction mechanisms and using this data regarding reaction mechanisms to inform predication-based carbon budget models. In this study, we broadly discuss reaction mechanisms, however, there are some limitations in quencher selectivity. This could potentially result in multiple PPRI being present at the same time and could make it more difficult to draw conclusions regarding quencher responsibility. In the future, experiments using multiple quenchers to quench multiple PPRI at the same time would inform reaction mechanisms attributed to specific PPRI more accurately. For example, reaction mechanisms such as hydroxylation or decarboxylation would be important to further analyze.

Additionally, it would be useful to construct a carbon budget model of indirect photolysis in diverse DOM pool. The construction of a carbon emissions model can be informed through dissolved gas measurements before and after photolysis along with FT-ICR MS measurements from quencher studies. Insights into carbon dioxide emissions from indirect photolysis can be found by using previous carbon budgets models and constructing part of a model relevant to inland lakes. Further, this can also give insights to reaction mechanisms that result in the most carbon

dioxide emissions. This would inform worldwide carbon budgets with important information to further understand greenhouse gas emissions and climate change.

Acknowledgements

This project was supported by the National Science Foundation (EAR-2104716). We acknowledge Noah Lottig and Alice Ogden-Nussbaum from the University of Wisconsin-Madison Trout Lake Research Station and the Hasler Laboratory of Limnology for facilitating sample collection through the support of the NTL-LTER program (NSF DEB-2025982). We acknowledge the UW-Madison Human Proteomics Program Mass Spectrometry Facility for support in obtaining mass spectrometry data, Yanlong Zhu for assistance with instrument operation, and NIH S10OD018475 for acquisition of the high-resolution mass spectrometer.

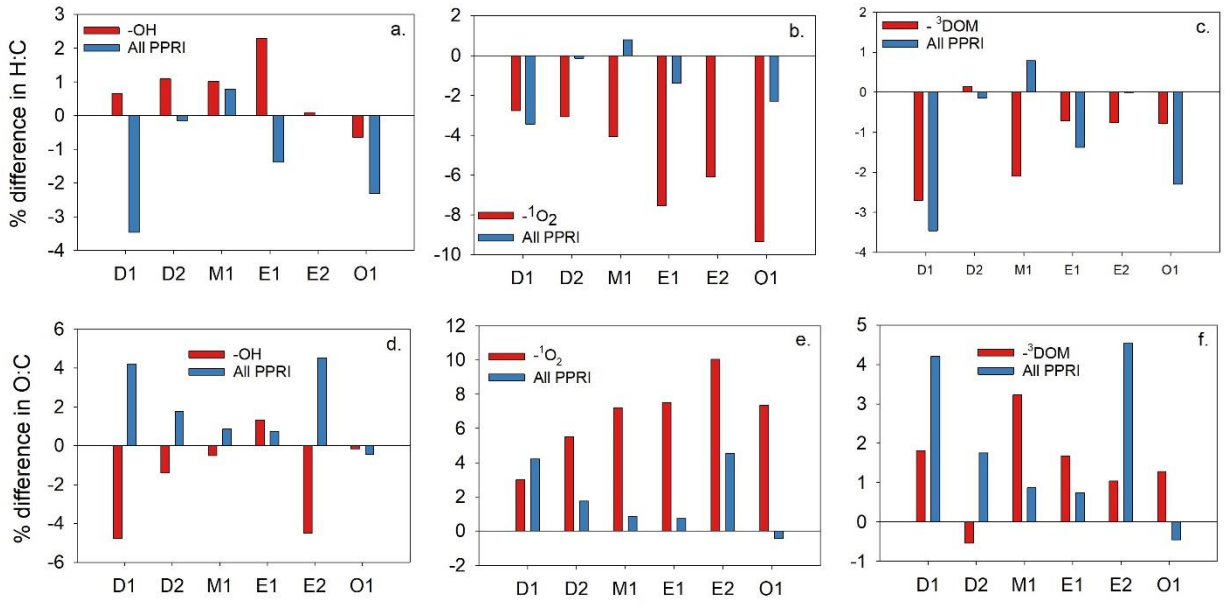

Figure 1: Percent difference in $H:C_w$ after irradiation for six DOM samples in the absence of quenchers (all PPRI) and in the presence of (a) TPA (-$^{\bullet}$OH), (b) FFA (-$^1O_2$), and (c) sorbic acid (-

^{3}DOM). Percent difference in O:C$_w$ after sample irradiation in the absence of quenchers (all PPRI) and in the presence of (d) TPA (-$^{\bullet}$OH), (e) FFA (-$^1O_2$), and (f) sorbic acid (-^{3}DOM). All percent differences are calculated relative to an unirradiated control with the same quencher.

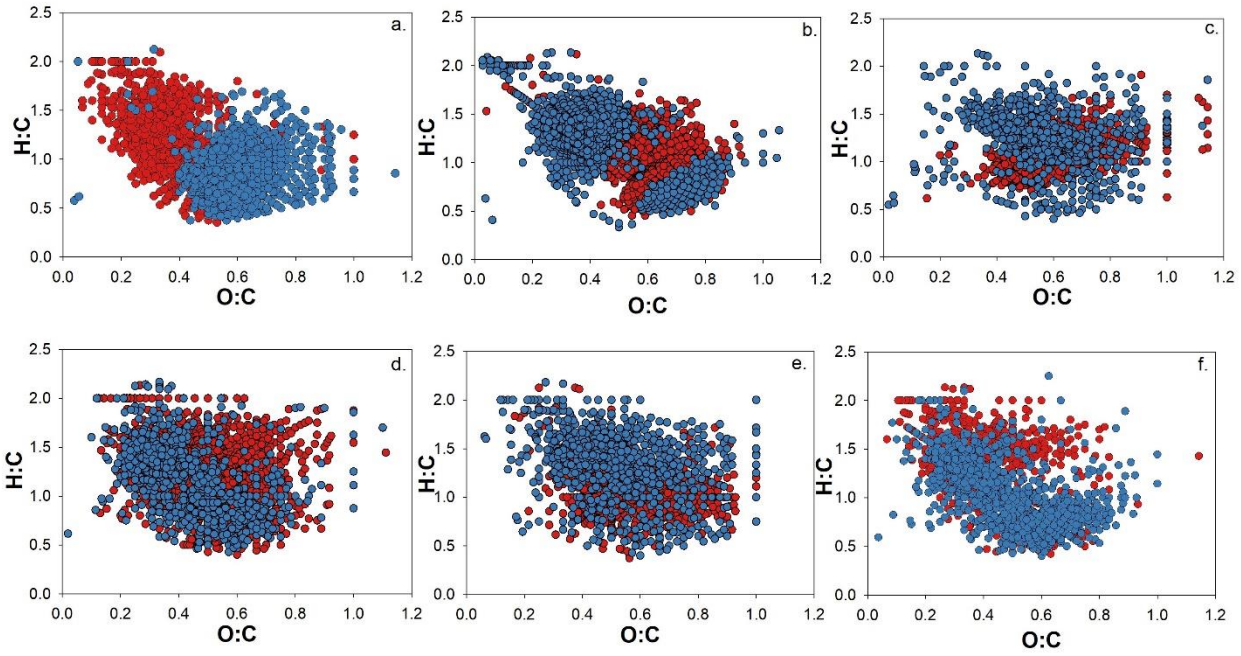

Figure 2: Relative intensity increases or decreases in the absence of specific PPRI compared to sample irradiated with no quenchers present. Red represents the sample treatment (a-b: -$^{\bullet}$OH, c-d: -$^1O_2$, e-f: -^{3}DOM) and blue represents the control (All PPRI) sample. The samples are organized by lake and the intensity change being measured (a) D1: Increasing, (b) D1: Decreasing, (c) E2: Increasing, (d) E2: Decreasing, (e) M1: Increasing, and (f) M1: Decreasing.

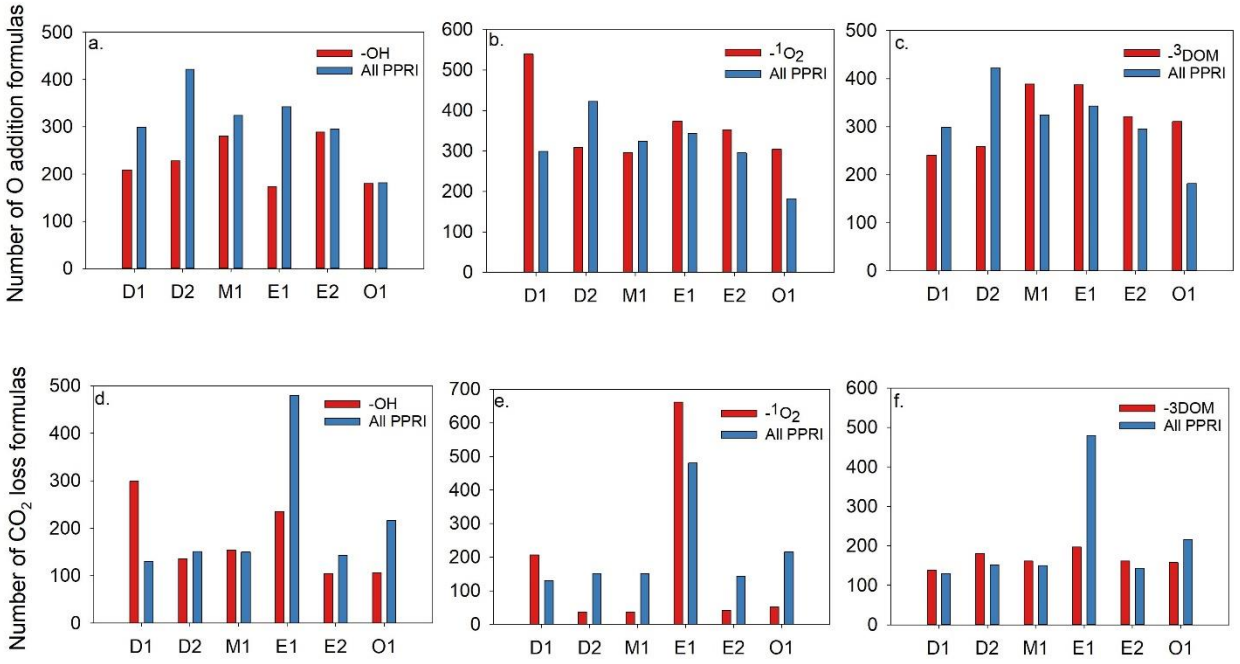

Figure 3: The number of (a-c) unique oxygen addition and (d-f) carbon dioxide loss formulas in the absence of specific PPRI compared to sample irradiated with no quenchers present.

References

(1) Battin, T. J.; Luyssaert, S.; Kaplan, L. A.; Aufdenkampe, A. K.; Richter, A.; Tranvik, L. J. The Boundless Carbon Cycle. *Nature Geoscience*. September 2009, pp 598–600. https://doi.org/10.1038/ngeo618.

(2) Buffam, I.; Turner, M. G.; Desai, A. R.; Hanson, P. C.; Rusak, J. A.; Lottig, N. R.; Stanley, E. H.; Carpenter, S. R. Integrating Aquatic and Terrestrial Components to Construct a Complete Carbon Budget for a North Temperate Lake District. *Global Change Biology* **2011**, *17* (2), 1193–1211. https://doi.org/10.1111/j.1365-2486.2010.02313.x.

(3) *Global Carbon Project (GCP). https://www.globalcarbonproject.org/carbonbudget/index.htm (accessed Apr 23, 2024).*

(4) Raymond, P. A.; Hartmann, J.; Lauerwald, R.; Sobek, S.; McDonald, C.; Hoover, M.; Butman, D.; Striegl, R.; Mayorga, E.; Humborg, C.; Kortelainen, P.; Dürr, H.; Meybeck, M.; Ciais, P.; Guth, P. Global Carbon Dioxide Emissions from Inland Waters. *Nature* **2013**, *503* (7476), 355–359. https://doi.org/10.1038/nature12760.

(5) Buffam, I.; Turner, M. G.; Desai, A. R.; Hanson, P. C.; Rusak, J. A.; Lottig, N. R.; Stanley, E. H.; Carpenter, S. R. Integrating Aquatic and Terrestrial Components to Construct a

Complete Carbon Budget for a North Temperate Lake District. *Global Change Biology* **2011**, *17* (2), 1193–1211. https://doi.org/10.1111/j.1365-2486.2010.02313.x.

(6) Ward, C. P.; Cory, R. M. Assessing the Prevalence, Products, and Pathways of Dissolved Organic Matter Partial Photo-Oxidation in Arctic Surface Waters. *Environmental Science Process Impacts* **2020**, *22* (5), 1214–1223. https://doi.org/10.1039/c9em00504h.

(7) Ward, C. P.; Cory, R. M. Complete and Partial Photo-Oxidation of Dissolved Organic Matter Draining Permafrost Soils. *Environmental Science Technology* **2016**, *50* (7), 3545–3553. https://doi.org/10.1021/acs.est.5b05354.

(8) Hu, A.; Jang, K. S.; Meng, F.; Stegen, J.; Tanentzap, A. J.; Choi, M.; Lennon, J. T.; Soininen, J.; Wang, J. Microbial and Environmental Processes Shape the Link between Organic Matter Functional Traits and Composition. *Environmental Science Technology* **2022**, *56* (14), 10504–10516. https://doi.org/10.1021/acs.est.2c01432.

(9) Liu, J.; Liang, J.; Bravo, A. G.; Wei, S.; Yang, C.; Wang, D.; Jiang, T. Anaerobic and Aerobic Biodegradation of Soil-Extracted Dissolved Organic Matter from the Water-Level-Fluctuation Zone of the Three Gorges Reservoir Region, China. *Science of the Total Environment* **2021**, *764*. https://doi.org/10.1016/j.scitotenv.2020.142857.

(10) Hur, J.; Park, M. H.; Schlautman, M. A. Microbial Transformation of Dissolved Leaf Litter Organic Matter and Its Effects on Selected Organic Matter Operational Descriptors. *Environmental Science Technology* **2009**, *43* (7), 2315–2321. https://doi.org/10.1021/es802773b.

(11) Cory, R.; Ward, C.; Crump, B.; Kling, G. Sunlight Controls Water Column of Carbon in Arctic Waters. *Science (1979)* **2014**, *345* (6199), 925–928. https://doi.org/10.1126/science.1255006.

(12) Spencer, R. G. M.; Stubbins, A.; Hernes, P. J.; Baker, A.; Mopper, K.; Aufdenkampe, A. K.; Dyda, R. Y.; Mwamba, V. L.; Mangangu, A. M.; Wabakanghanzi, J. N.; Six, J. Photochemical Degradation of Dissolved Organic Matter and Dissolved Lignin Phenols from the Congo River. *Geophysical Research Biogeoscience* **2009**, *114* (3). https://doi.org/10.1029/2009JG000968.

(13) Gonsior, M.; Schmitt-Kopplin, P.; Bastviken, D. Depth-Dependent Molecular Composition and Photo-Reactivity of Dissolved Organic Matter in a Boreal Lake under Winter and Summer Conditions. *Biogeosciences* **2013**, *10* (11), 6945–6956. https://doi.org/10.5194/bg-10-6945-2013.

(14) Lou, T.; Xie, H. Photochemical Alteration of the Molecular Weight of Dissolved Organic Matter. *Chemosphere* **2006**, *65* (11), 2333–2342. https://doi.org/10.1016/j.chemosphere.2006.05.001.

(15) Gonsior, M.; Hertkorn, N.; Conte, M. H.; Cooper, W. J.; Bastviken, D.; Druffel, E.; Schmitt-Kopplin, P. Photochemical Production of Polyols Arising from Significant Photo-Transformation of Dissolved Organic Matter in the Oligotrophic Surface Ocean. *Marine Chemistry* **2014**, *163*, 10–18. https://doi.org/10.1016/j.marchem.2014.04.002.

(16) Sharpless, C. M.; Aeschbacher, M.; Page, S. E.; Wenk, J.; Sander, M.; McNeill, K. Photooxidation-Induced Changes in Optical, Electrochemical, and Photochemical Properties of Humic Substances. *Environmental Science Technology* **2014**, *48* (5), 2688–2696. https://doi.org/10.1021/es403925g.

(17) Mann, P. J.; Davydova, A.; Zimov, N.; Spencer, R. G. M.; Davydov, S.; Bulygina, E.; Zimov, S.; Holmes, R. M. Controls on the Composition and Lability of Dissolved Organic Matter in Siberia's Kolyma River Basin. *Geophysical Research Biogeoscience* **2012**, *117* (1). https://doi.org/10.1029/2011JG001798.

(18) Helms, J. R.; Stubbins, A.; Ritchie, J. D.; Minor, E. C.; Kieber, D. J.; Mopper, K. Absorption Spectral Slopes and Slope Ratios as Indicators of Molecular Weight, Source, and Photobleaching of Chromophoric Dissolved Organic Matter. *Limnology Oceanography* **2008**, *53* (3), 955–969. https://doi.org/10.4319/lo.2008.53.3.0955.

(19) Ward, C. P.; Nalven, S. G.; Crump, B. C.; Kling, G. W.; Cory, R. M. Photochemical Alteration of Organic Carbon Draining Permafrost Soils Shifts Microbial Metabolic Pathways and Stimulates Respiration. *Nature Communications* **2017**, *8* (1). https://doi.org/10.1038/s41467-017-00759-2.

(20) Ward, C. P.; Sleighter, R. L.; Hatcher, P. G.; Cory, R. M. Insights into the Complete and Partial Photooxidation of Black Carbon in Surface Waters. *Environmental Sciences: Processes and Impacts* **2014**, *16* (4), 721–731. https://doi.org/10.1039/c3em00597f.

(21) Gonsior, M.; Peake, B. M.; Cooper, W. T.; Podgorski, D.; D'Andrilli, J.; Cooper, W. J. Photochemically Induced Changes in Dissolved Organic Matter Identified by Ultrahigh Resolution Fourier Transform Ion Cyclotron Resonance Mass Spectrometry. *Environmental Science Technology* **2009**, *43* (3), 698–703. https://doi.org/10.1021/es8022804.

(22) Stubbins, A.; Spencer, R. G. M.; Chen, H.; Hatcher, P. G.; Mopper, K.; Hernes, P. J.; Mwamba, V. L.; Mangangu, A. M.; Wabakanghanzi, J. N.; Six, J. Illuminated Darkness: Molecular Signatures of Congo River Dissolved Organic Matter and Its Photochemical Alteration as Revealed by Ultrahigh Precision Mass Spectrometry. *Limnology Oceanography* **2010**, *55* (4), 1467–1477. https://doi.org/10.4319/lo.2010.55.4.1467.

(23) Berg, S. M.; Wammer, K. H.; Remucal, C. K. Dissolved Organic Matter Photoreactivity Is Determined by Its Optical Properties, Redox Activity, and Molecular Composition.

Environmental Science Technology **2023**, *57* (16), 6703–6711. https://doi.org/10.1021/acs.est.3c01157.

(24) Milstead, R. P.; Horvath, E. R.; Remucal, C. K. Dissolved Organic Matter Composition Determines Its Susceptibility to Complete and Partial Photooxidation within Lakes. *Environmental Science Technol*ogy **2023**, *57* (32), 11876–11885. https://doi.org/10.1021/acs.est.3c01500.

(25) McNeill, K.; Canonica, S. Triplet State Dissolved Organic Matter in Aquatic Photochemistry: Reaction Mechanisms, Substrate Scope, and Photophysical Properties. *Environmental Science Process Impacts* **2016**, *18* (11), 1381–1399. https://doi.org/10.1039/c6em00408c.

(26) Goldstone, J. V.; Pullin, M. J.; Bertilsson, S.; Voelker, B. M. Reactions of Hydroxyl Radical with Humic Substances: Bleaching, Mineralization, and Production of Bioavailable Carbon Substrates. *Environmental Science Technology* **2002**, *36* (3), 364–372. https://doi.org/10.1021/es0109646.

(27) Cory, R. M.; McNeill, K.; Cotner, J. P.; Amado, A.; Purcell, J. M.; Marshall, A. G. Singlet Oxygen in the Coupled Photochemical and Biochemical Oxidation of Dissolved Organic Matter. *Environmental Science Technology* **2010**, *44* (10), 3683–3689. https://doi.org/10.1021/es902989y.

(28) Rosario-Ortiz, F. L.; Canonica, S. Probe Compounds to Assess the Photochemical Activity of Dissolved Organic Matter. *Environmental Science Technology* **2016**.

(29) Remucal, C. K. The Role of Indirect Photochemical Degradation in the Environmental Fate of Pesticides: A Review. *Environmental Sciences: Processes and Impacts*. Royal Society of Chemistry 2014, pp 628–653. https://doi.org/10.1039/c3em00549f.

(30) Cory, R. M.; Cotner, J. B.; Mcneill, K. Quantifying Interactions between Singlet Oxygen and Aquatic Fulvic Acids. *Environmental Science Technology* **2009**, *43* (3), 718–723. https://doi.org/10.1021/es801847g.

(31) Waggoner, D. C.; Wozniak, A. S.; Cory, R. M.; Hatcher, P. G. The Role of Reactive Oxygen Species in the Degradation of Lignin Derived Dissolved Organic Matter. *Geochimica Cosmochimica Acta* **2017**, *208*, 171–184. https://doi.org/10.1016/j.gca.2017.03.036.

(32) Pullin, M. J.; Bertilsson, S.; Goldstone, J. V; Voelker, B. M. Effects of Sunlight and Hydroxyl Radical on Dissolved Organic Matter: Bacterial Growth Efficiency and Production of Carboxylic Acids and Other Substrates. *Limnology Oceanography* **2004**, *49* (6), 2011–2022.

(33) Page, S. E.; Logan, J. R.; Cory, R. M.; McNeill, K. Evidence for Dissolved Organic Matter as the Primary Source and Sink of Photochemically Produced Hydroxyl Radical in Arctic Surface Waters. *Environmental Sciences: Processes and Impacts* **2014**, *16* (4), 807–822. https://doi.org/10.1039/c3em00596h.

(34) https://lter.limnology.wisc.edu/. *North Temperate Lakes US Long-Term Ecological Research Network*.

(35) Weishaar, J. L.; Aiken, G. R.; Bergamaschi, B. A.; Fram, M. S.; Fujii, R.; Mopper, K. Evaluation of Specific Ultraviolet Absorbance as an Indicator of the Chemical Composition and Reactivity of Dissolved Organic Carbon. *Environmental Science Technology* **2003**, *37* (20), 4702–4708. https://doi.org/10.1021/es030360x.

(36) Helms, J. R.; Stubbins, A.; Ritchie, J. D.; Minor, E. C.; Kieber, D. J.; Mopper, K. Absorption Spectral Slopes and Slope Ratios as Indicators of Molecular Weight, Source, and Photobleaching of Chromophoric Dissolved Organic Matter. *Limnology Oceanography* **2008**, *53* (3), 955–969.

(37) Mcknight, D. M.; Boyer, E. W.; Westerhoff, P. K.; Doran, P. T.; Kulbe, T.; Andersen, D. T. Spectrofluorometric Characterization of Dissolved Organic Matter for Indication of Precursor Organic Material and Aromaticity; 2001; Vol. 46.

(38) Ohno, T. Fluorescence Inner-Filtering Correction for Determining the Humification Index of Dissolved Organic Matter. *Environmental Science Technology* **2002**, *36* (4), 742–746. https://doi.org/10.1021/es0155276.

(39) Huguet, A.; Vacher, L.; Relexans, S.; Saubusse, S.; Froidefond, J. M.; Parlanti, E. Properties of Fluorescent Dissolved Organic Matter in the Gironde Estuary. *Organic Geochemistry* **2009**, *40* (6), 706–719. https://doi.org/10.1016/j.orggeochem.2009.03.002.

(40) Bulman, D. M.; Mezyk, S. P.; Remucal, C. K. The Impact of PH and Irradiation Wavelength on the Production of Reactive Oxidants during Chlorine Photolysis. *Environmental Science Technology* **2019**, *53* (8), 4450–4459. https://doi.org/10.1021/acs.est.8b07225.

(41) Laszakovits, J. R.; Berg, S. M.; Anderson, B. G.; O'Brien, J. E.; Wammer, K. H.; Sharpless, C. M. P-Nitroanisole/Pyridine and p-Nitroacetophenone/Pyridine Actinometers Revisited: Quantum Yield in Comparison to Ferrioxalate. *Environmental Science Technology Letters* **2017**, *4* (1), 11–14. https://doi.org/10.1021/acs.estlett.6b00422.

(42) Maizel, A. C.; Remucal, C. K. Molecular Composition and Photochemical Reactivity of Size-Fractionated Dissolved Organic Matter. *Environmental Science Technology* **2017**, *51* (4), 2113–2123. https://doi.org/10.1021/acs.est.6b05140.

(43) Maizel, A. C.; Remucal, C. K. The Effect of Probe Choice and Solution Conditions on the Apparent Photoreactivity of Dissolved Organic Matter. *Environmental Science Process Impacts* **2017**, *19* (8), 1040–1050. https://doi.org/10.1039/c7em00235a.

(44) Bulman, D. M.; Remucal, C. K. Role of Reactive Halogen Species in Disinfection Byproduct Formation during Chlorine Photolysis. *Environmental Science Technology* **2020**, *54* (15), 9629–9639. https://doi.org/10.1021/acs.est.0c02039.

(45) Gonsior, M.; Schmitt-Kopplin, P.; Stavklint, H.; Richardson, S. D.; Hertkorn, N.; Bastviken, D. Changes in Dissolved Organic Matter during the Treatment Processes of a Drinking Water Plant in Sweden and Formation of Previously Unknown Disinfection Byproducts. *Environmental Science Technology* **2014**, *48* (21), 12714–12722. https://doi.org/10.1021/es504349p.

(46) Ziegler, G.; Gonsior, M.; Fisher, D. J.; Schmitt-Kopplin, P.; Tamburri, M. N. Formation of Brominated Organic Compounds and Molecular Transformations in Dissolved Organic Matter (Dom) after Ballast Water Treatment with Sodium Dichloroisocyanurate Dihydrate (DICD). *Environmental Science Technology* **2019**, *53* (14), 8006–8016. https://doi.org/10.1021/acs.est.9b01064.

(47) Maizel, A. C.; Li, J.; Remucal, C. K. Relationships between Dissolved Organic Matter Composition and Photochemistry in Lakes of Diverse Trophic Status. *Environmental Science Technology* **2017**, *51* (17), 9624–9632. https://doi.org/10.1021/acs.est.7b01270.

(48) Berg, S. M.; Whiting, Q. T.; Herrli, J. A.; Winkels, R.; Wammer, K. H.; Remucal, C. K. The Role of Dissolved Organic Matter Composition in Determining Photochemical Reactivity at the Molecular Level. *Environmental Science Technology* **2019**, *53* (20), 11725–11734. https://doi.org/10.1021/acs.est.9b03007.

(49) Koch, B. P.; Witt, M.; Engbrodt, R.; Dittmar, T.; Kattner, G. Molecular Formulae of Marine and Terrigenous Dissolved Organic Matter Detected by Electrospray Ionization Fourier Transform Ion Cyclotron Resonance Mass Spectrometry. *Geochimica Cosmochimica Acta* **2005**, *69* (13), 3299–3308. https://doi.org/10.1016/j.gca.2005.02.027.

(50) Hansen, A. M.; Kraus, T. E. C.; Pellerin, B. A.; Fleck, J. A.; Downing, B. D.; Bergamaschi, B. A. Optical Properties of Dissolved Organic Matter (DOM): Effects of Biological and Photolytic Degradation. *Limnology Oceanography* **2016**, *61* (3), 1015–1032. https://doi.org/10.1002/lno.10270.

(51) Maizel, A. C.; Li, J.; Remucal, C. K. Relationships between Dissolved Organic Matter Composition and Photochemistry in Lakes of Diverse Trophic Status. *Environmental Science Technology* **2017**, *51* (17), 9624–9632. https://doi.org/10.1021/acs.est.7b01270.

(52) Minor, E.; Stephens, B. Dissolved Organic Matter Characteristics within the Lake Superior Watershed. *Orgic Geochemistry* **2008**, *39* (11), 1489–1501. https://doi.org/10.1016/j.orggeochem.2008.08.001.

(53) Helms, J. R.; Stubbins, A.; Perdue, E. M.; Green, N. W.; Chen, H.; Mopper, K. Photochemical Bleaching of Oceanic Dissolved Organic Matter and Its Effect on Absorption Spectral Slope and Fluorescence. *Marine Chemistry* **2013**, *155*, 81–91. https://doi.org/10.1016/j.marchem.2013.05.015.

(54) Zsolnay', A.; Baigar, E.; Jimenez', M.; Steinweg', B.; Saccomandi', F. Differentiating with Fluorescence Spectroscopy the Sources of Dissolved Organic Matter in Soils Subjected to Drying. *Chemosphere* **1999**, *38* (1), 45–50.

(55) McKnight, D. M.; Boyer, E. W.; Westerhoff, P. K.; Doran, P. T.; Kulbe, T.; Andersen, D. T. Spectrofluorometric Characterization of Dissolved Organic Matter for Indication of Precursor Organic Material and Aromaticity. *Limnology Oceanography* **2001**, *46* (1), 38–48. https://doi.org/10.4319/lo.2001.46.1.0038.

(56) Herzsprung, P.; Wentzky, V.; Kamjunke, N.; Von Tümpling, W.; Wilske, C.; Friese, K.; Boehrer, B.; Reemtsma, T.; Rinke, K.; Lechtenfeld, O. J. Improved Understanding of Dissolved Organic Matter Processing in Freshwater Using Complementary Experimental and Machine Learning Approaches. *Environmental Science Technology* **2020**, *54* (21), 13556–13565. https://doi.org/10.1021/acs.est.0c02383.

(57) Li, S. A.; Wang, Q.; Ma, H.; Cao, X.; Song, Y.; Cui, F.; Tanentzap, A. J. Photochemical Processes Transform Dissolved Organic Matter Differently Depending on Its Initial Composition. *Science of the Total Environment* **2024**, *923*. https://doi.org/10.1016/j.scitotenv.2024.171465.

(58) Remucal, C. K.; Salhi, E.; Walpen, N.; Von Gunten, U. Molecular-Level Transformation of Dissolved Organic Matter during Oxidation by Ozone and Hydroxyl Radical. *Environmental Science Technology* **2020**, *54* (16), 10351–10360. https://doi.org/10.1021/acs.est.0c03052.

(59) Schollée, J. E.; Bourgin, M.; von Gunten, U.; McArdell, C. S.; Hollender, J. Non-Target Screening to Trace Ozonation Transformation Products in a Wastewater Treatment Train Including Different Post-Treatments. *Water Research* **2018**, *142*, 267–278. https://doi.org/10.1016/j.watres.2018.05.045.

(60) Von Gunten, U. *Ozonation of Drinking Water: Part I. Oxidation Kinetics and Product Formation*; 2003; Vol. 37.

(61) Cory, R. M.; McNeill, K.; Cotner, J. P.; Amado, A.; Purcell, J. M.; Marshall, A. G. Singlet Oxygen in the Coupled Photochemical and Biochemical Oxidation of Dissolved Organic

Matter. *Environmental Science Technology* **2010**, *44* (10), 3683–3689. https://doi.org/10.1021/es902989y.

(62) Li, S. A.; Wang, Q.; Ma, H.; Cao, X.; Song, Y.; Cui, F.; Tanentzap, A. J. Photochemical Processes Transform Dissolved Organic Matter Differently Depending on Its Initial Composition. *Science of the Total Environment* **2024**, *923*. https://doi.org/10.1016/j.scitotenv.2024.171465.

(63) Schmitt, M.; Moor, K. J.; Erickson, P. R.; McNeill, K. Sorbic Acid as a Triplet Probe: Reactivity of Oxidizing Triplets in Dissolved Organic Matter by Direct Observation of Aromatic Amine Oxidation. *Environmental Science Technology* **2019**, *53* (14), 8087–8096. https://doi.org/10.1021/acs.est.9b01789.

(64) Kong, Q.; Ye, L.; Pan, Y.; Zhou, Y.; Lei, Y.; Zeng, Z.; Chen, S.; Yao, L.; Zhang, X.; Westerhoff, P.; Yang, X. Photochemical Transformation of Free Chlorine Induced by Triplet State Dissolved Organic Matter. *Environmental Science Technology* **2023**, *57* (29), 10849–10859. https://doi.org/10.1021/acs.est.3c02458.

(65) Kong, Q.; Pan, Y.; Lei, X.; Zhou, Y.; Lei, Y.; Peng, J.; Zhang, X.; Yin, R.; Shang, C.; Yang, X. Reducing Properties of Triplet State Organic Matter (3DOM*) Probed via the Transformation from Chlorine Dioxide to Chlorite. *Water Research* **2022**, *225*. https://doi.org/10.1016/j.watres.2022.119120.

(66) Wenk, J.; Von Gunten, U.; Canonica, S. Effect of Dissolved Organic Matter on the Transformation of Contaminants Induced by Excited Triplet States and the Hydroxyl Radical. *Environmental Science Technology* **2011**, *45* (4), 1334–1340. https://doi.org/10.1021/es102212t.

(67) Wu, B.; Arnold, W. A.; Ma, L. Photolysis of Atrazine: Role of Triplet Dissolved Organic Matter and Limitations of Sensitizers and Quenchers. *Water Research* **2021**, *190*. https://doi.org/10.1016/j.watres.2020.116659.

(68) Gerecke, A. C.; Canonica, S.; Muller, S. R.; Scharer, M.; Schwarzenbach, R. P. Quantification of Dissolved Natural Organic Matter (DOM) Mediated Phototransformation of Phenylurea Herbicides in Lakes. *Environmental Science Technology* **2001**, *35* (19), 3915–3923. https://doi.org/10.1021/es010103x.

(69) Canonica, S.; Jans, U.; Stemmler, K.; Hoigné, J. Transformation Kinetics of Phenols in Water: Photosensitization by Dissolved Natural Organic Material and Aromatic Ketones; 1995; Vol. 29. https://pubs.acs.org/sharingguidelines.

Appendix A. Supplemental Information for Chapter 1

Section S1: Chemicals

Methanol (MeOH; ACS Reagent Grade, ≥99.8%), sodium hydroxide (reagent grade), sorbic acid (SA) (>99%), and 2-hydroxyterephthalic acid (>97%) were purchased from Sigma Aldrich. Acetonitrile (HPLC grade), hydrochloric acid (concentrated, ACS grade), formic acid (ACS, 88%), sodium bicarbonate (Certified ACS Grade), 2-propanol (IPA), sulfuric acid (Trace Metal Grade), potassium hydrogen phthalate (ACS grade), and *ortho*-phosphoric acid (ACS, 98%) were purchased from Fisher Chemical. *para*-Nitroanisole (>99%) was purchased from Acros Organics. 2,4,6-Trimethylphenol (>98%) and Pyridine (>99%) were purchased from Alfa Aesar. Sodium terephthalate was purchased from MP biomedicals LLC. Furfuryl alcohol (>97%) was purchased from Tokyo Chemical Industry (TCI). Ultrapure water (18.2 MΩ cm) was obtained from a Milli-Q water purification system.

Section S2: Sample Locations

Samples were collected from core lakes from the North Temperate Lakes Long Term Ecological Research (NTL-LTER) sites (**Table S1**).[34] These sites included lakes of diverse trophic levels and DOM composition. Water samples were taken from the middle of the lake in the top one meter of the water column. After collection, the samples were filtered with a 0.45 μm glass fiber filters within 72 hours and stored in the dark at 4˚C.

Table S1: Information regarding the sample waters collected in November of 2022.

Sample	Coordinates	Description	Sample label
Trout Bog	46.041, -89.686	Dystrophic Lake	D1
Crystal Bog	46.008, -89.606	Dystrophic Lake	D2
Allequash Lake	46.038, -89.621	Mesotrophic Lake	M1
Lake Monona	43.063, -89.361	Eutrophic Lake	E1
Fish Lake	43.287, -89.652	Eutrophic Lake	E2
Lake Mendota	43.099, -89.405	Eutrophic Lake	E3
Lake Wingra	43.053, -89.425	Eutrophic Lake	E4
Big Muskellunge Lake	46.021, -89.612	Oligotrophic Lake	O1
Crystal Lake	46.003, -89.612	Oligotrophic Lake	O2
Sparkling Lake	46.008, -89.701	Oligotrophic Lake	O3
Trout Lake	46.029, -89.665	Oligotrophic Lake	O4

Section S3: Water chemistry and bulk characteristics

pH measurements were done using a Mettler Toledo EL20 pH meter (**Table S2**). Dissolved organic carbon concentrations ([DOC]) were taken using a Shimadzu Total Organic Carbon Analyzer (**Table S2**). The TOC analyzer was calibrated externally with a potassium hydrogen phthalate standard.

Table S2: Basic water chemistry parameters

Sample	[DOC] (mg-C L^{-1})	pH
Trout Bog (D1)	25.6 ± 0.05	5.50 ± 0.10
Crystal Bog (D2)	9.19 ± 0.03	6.07 ± 0.10
Allequash Lake (M1)	4.70 ± 0.01	7.84 ± 0.10
Lake Monona (E1)	4.63 ± 0.05	8.15 ± 0.10
Fish Lake (E2)	6.10 ± 0.08	8.06 ± 0.10

Lake Mendota (E3)	4.67 ± 0.21	8.03 ± 0.10
Lake Wingra (E4)	6.53 ± 0.05	8.06 ± 0.10
Big Muskellunge Lake (O1)	5.33 ± 0.04	8.02 ± 0.10
Crystal Lake (O2)	3.04 ± 0.01	7.75 ± 0.10
Sparkling Lake (O3)	4.51 ± 0.04	7.61 ± 0.10
Trout Lake (O4)	3.33 ± 0.02	7.63 ± 0.10

Concentrations of anions including nitrate, sulfate, and chloride, were measured using anion exchange chromatography (**Table S3.1**) using a Dionex ICS-2100 instrument and a Dionex IonPac AS11-HC RFIC^{TM} column (4 x 250mm) with a guard column (4 x 50 mm). The limits of detection were 0.5 ppm for nitrate, 0.8 ppm for chloride and 0.6 ppm for sulfate. The concentrations of cations including calcium, magnesium, and iron were measured as part of the North Temperature Lakes-Long Term Ecological Research program.[34] Cation concentrations from August of 2022 were listed here to give general overview of cation concentrations closest to the sampling date (**Table S3.2**).

Table S3.1: Measured anion concentration in sample waters.

Sample	**[NO_3^-] (ppm)**	**[Cl^-] (ppm)**	**[SO_4^{3-}] (ppm)**
Trout Bog	<0.5	<0.8	<0.6
Crystal Bog	<0.5	<0.8	<0.6
Allequash Lake	<0.5	<0.8	1.4
Lake Monona	<0.5	63.6	10.8
Fish Lake	0.6	7.3	<0.6
Lake Mendota	<0.5	48.3	11.1
Lake Wingra	<0.5	114.1	14.0
Big Muskellunge Lake	<0.5	<0.8	1.2
Crystal Lake	<0.5	<0.8	1
Sparkling Lake	<0.5	10.6	1.1
Trout Lake	<0.5	0.94	1.3

Table S3.2: Selected cation concentrations in sample waters from the NTL-LTER public dataset during August of 2022. *Fish Lake most recent data was from March 2022. **The most recent data from Lake Mendota, Lake Monona, and Lake Wingra were from February 2022.

Sample	[Ca^{2+}] (ppm)	[Mg^{2+}] (ppm)	[Dissolved Fe] (ppm)
Trout Bog	1.1	0.3	0.23
Crystal Bog	0.7	0.2	0.36
Allequash Lake	12.1	3.4	<0.02
Lake Monona**	36.8	36.5	<0.02
Fish Lake*	32.9	22.5	<0.02
Lake Mendota**	37.0	37.4	<0.02
Lake Wingra**	79.1	52.1	<0.02
Big Muskellunge Lake	6.7	2.1	<0.02
Crystal Lake	1.0	0.27	<0.02
Sparkling Lake	11.7	3.5	<0.02
Trout Lake	13.0	3.4	<0.02

General bulk DOM characteristics were collected using UV-vis spectrometry and fluorescence spectroscopy. UV-vis spectra were collected on Shimadzu UV-visible spectrometer and was analyzed from 200-800 nm and 1 cm pathlength. Fluorescence spectroscopy was analyzed on a Horiba Aqualog and an excitation emission matrix was produced from 250-800 nm. The data was corrected for inner filter effects and Rayleigh scattering. From UV-Vis spectroscopy results, $SUVA_{254}$ and E_2:E_3 were calculated as seen in **Table S4**. From fluorescence spectroscopy results, fluorescence indices (FI) and biological indices (BIX) were calculated as seen in **Table S4**.[55,70–72] $SUVA_{254}$, E_2:E_3, FI, and BIX results for all sample waters were included in **Table S5**.

Table S4: Calculations for various bulk water chemistry parameters

Parameter	Calculation
$SUVA_{254}$	$\frac{Abs.\ 254\ nm}{[DOC]}$ x 1000
E_2:E_3	$\frac{Abs.250\ nm}{Abs.365\ nm}$

Fluorescence Index (FI)	= em. $\frac{470\ nm}{520\ nm}$ at ex. 370 nm
Biological Index (BIX)	= em. $\frac{380\ nm}{430\ nm}$ at ex. 310 nm

Table S5: Bulk water chemistry parameters from sample waters.

Sample	$SUVA_{254}$ (L mg-C^{-1} m^{-1})	E_2:E_3	FI	BIX
Trout Bog (D1)	5.87	4.47	1.38	0.46
Crystal Bog (D2)	2.94	5	1.43	0.50
Allequash Lake (M1)	2.01	6.46	1.52	0.75
Lake Monona (E1)	1.82	10.6	1.70	0.98
Fish Lake (E2)	1.5	10.8	1.63	1.03
Lake Mendota (E3)	1.69	10.8	1.63	0.97
Lake Wingra (E4)	1.99	7.71	1.61	0.89
Big Muskellunge Lake (O1)	0.75	9.75	1.61	0.88
Crystal Lake (O2)	0.61	10	1.67	0.95
Sparkling Lake (O3)	1.11	10.6	1.58	0.86
Trout Lake (O4)	1.35	9.9	1.63	0.85

Section S4: Photochemistry experiments

Photochemistry experiments were performed to quantify the concentration of photochemically produced reactive intermediates (PPRI) in the sample waters. Probe molecules (10 μM) were used to quantify specific PPRI including 2,4,6-trimethylphenol (TMP) to quantify ^{3}DOM, furfuryl alcohol (FFA) to quantify $^1O_2$, and sodium terephthalate (TPA) to quantify $^{\bullet}$OH. These photochemical probe experiments were done in a Rayonet photoreactor with 365 nm bulbs at room temperature. The irradiation times ranged from 2-4 hours allowing 6-8 time points

throughout the experiment. Probe molecules TMP and FFA followed first order degradation kinetics while TPA was used to measure the formation of 2-hydroxyterephalic acid (hTPA).[43,73]

The degradation and formation of these probe molecules as well as a *p*-nitroanisole/pyridine actinometer were measured with high performance liquid chromatography (HPLC) using an Agilent 1260 with a 1260 diode array detector and a 1260 fluorescence detector.[41] The analyte, column, eluent, and detector used are listed in **Table S6**.

Table S6: HPLC methods for probe compounds and PNA. Type of analyte, column, eluent, and detectors (DAD: diode array detector and FLD: fluorescence detector) are listed for each analyte and PNA.

Analyte	**Column**	**Eluent**	**Detection**
p-Nitroanisole (PNA)	Agilent Poroshell 120 EC-C18 (3.0 x 50 mm)	65:35 0.1% Formic acid with 10% acetonitrile: acetonitrile	DAD at 314 nm
Furfuryl alcohol (FFA)	Agilent Poroshell 120 EC-C18 (3.0 x 50 mm)	90:10 0.1% Formic acid with 10% acetonitrile: acetonitrile	DAD at 217 nm
2, 4, 6-Trimethylphenol (TMP)	Agilent Poroshell 120 EC-C18 (3.0 x 50 mm)	50:50 0.1% Formic acid with 10% acetonitrile: acetonitrile	FLD: excitation at 230 nm, emission at 325 nm
Sodium Terephthalate (TPA)	Agilent Poroshell 120 Bonus RP (3.0 x 100 mm)	60:40 0.1% Phosphoric acid: acetonitrile	FLD: excitation at 250 nm, emission at 410 nm

Steady-state concentrations. For the steady-state concentration of ^{3}DOM, the measured pseudo-first-order rate constant ($k_{obs,TMP}$) was divided by $k_{TMP,3DOM}$ (second-order rate constant for the reaction between ^{3}DOM and TMP; 2.6 x 10^{-9} M^{-1} s^{-1}) as seen in **Table S7**.[43] These experiments were conducted at a normalized [DOC] of 3 mg-C L^{-1} as seen previously.[43]

The steady-state concentration of $^1O_2$ was measured by dividing the pseudo-first-order rate constant ($k_{obs,FFA}$) by the rate constant $k_{FFA,1O2}$ between $^1O_2$ and FFA (1.00 x 10^8 M^{-1} s^{-1}) as seen in **Table S7**.[42,74]

Finally, the steady-state concentration of •OH was calculated using the formation rate of hTPA ($k_{obs,TPA}$) and $k_{TPA,OH}$ as the rate constant for the reaction between hydroxyl radical and TPA (4.4 x 10^9 M^{-1} s^{-1}) as seen in **Table S7**.[73]

Quantum yields. Quantum yields were calculated for $^1O_2$ and •OH, while a quantum yield coefficient was calculated for ^{3}DOM. The quantum yield of singlet oxygen formation (Φ_{1O2}) was calculated as described previously using the equation in **Table S7**.[42] The equation used variables including Φ_{PNA}, $[PNA]_{t=0}$, $k_{obs\ PNA}$, the rate constant for quenching of $^1O_2$ by water (k_d, 2.4 x 10^5 s^{-1}), k_{FFA}, the rate of light absorption of both PNA ($R_{a,PNA}$) and FFA ($R_{a,FFA}$), and the observed rate constant of degradation of FFA ($k_{obs,FFA}$).[43,74]

The quantum yield coefficient of triplet DOM was also calculated like previous studies using the equation presented in **Table S7**. Quantum yield coeffecients were calculated here because The variables used were like singlet oxygen and include $\Phi_{PNA,}$ $[PNA]_{t=0}$, $k_{obs,\ PNA}$, $R_{a,\ PNA}$, and the rate of light absorption of TMP ($R_{a,\ TMP}$).[51,69]

Finally, the quantum yield of hydroxyl radical was calculated like previous studies using the equation presented in **Table S7**. The equation used $[•OH]_{ss}$, $R_{a,\ TPA}$, $[HCO_3^-]$, $[CO_3^{2-}]$, and [DOC] found experimentally and constants including $k_{•OH,HCO3}$ = 8.5 x 10^6 M^{-1} s^{-1}, $k_{•OH,CO3}$ = 3.9 x 10^8 M^{-1} s^{-1}, and $k_{•OH,DOM}$ = 1.9 x 10^4 mg-C^{-1} L s^{-1}.[23,75,76]

Table S7: Summary of equations needed for steady-state and quantum yield calculations.

PPRI	Steady-state concentration	Quantum yield
^{3}DOM	$[^3DOM]_{ss} = \frac{k_{obs,TMP}}{k_{TMP}}$	$f_{TMP} = \frac{\Phi_{PNA}}{[PNA]_{t=0}} \times \frac{R_{a,PNA}}{R_{a,TMP}} \times \frac{k_{obs,TMP}}{k_{obs,PNA}}$
$^1O_2$	$[^1O_2]_{ss} = \frac{k_{obs,FFA}}{k_{FFA}}$	$\Phi_{1O2} = \frac{\Phi_{PNA}}{[PNA]_{t=0}} \times \frac{R_{a,PNA}}{R_{a,FFA}} \times \frac{(k_{obs,FFA} \times k_d)}{(k_{obs,PNA} \times k_{FFA})}$
$^{\bullet}$OH	$[^{\bullet}OH]_{ss} = \frac{k_{obs,TPA}}{k_{TPA}}$	$\Phi_{\bullet OH} = \frac{k_{\bullet OH,HCO3}[HCO_3^-] + k_{\bullet OH,CO3}[CO_3^{2-}] + k_{\bullet OH,[DOC]}[DOC][\bullet OH]_{ss}}{R_a}$

Table S8: Steady-state concentrations for the sample waters. Error represents standard deviation in triplicate measurements.

Sample	$[^3DOM]_{ss}$ (M)	$[^1O_2]_{ss}$ (M)	$[^{\bullet}OH]_{ss}$ (M)
Trout Bog	(3.9 ± 0.18) x 10^{-14}	(9.3 ± 0.20) x 10^{-13}	(1.8 ± 0.01) x 10^{-15}
Crystal Bog	(3.0 ± 0.20) x 10^{-14}	(3.6 ± 0.04) x 10^{-13}	(9.5 ± 2.0) x 10^{-17}
Allequash Lake	(3.1 ± 0.05) x 10^{-14}	(2.3 ± 0.20) x 10^{-13}	(1.7 ± 0.30) x 10^{-16}
Lake Monona	(4.6 ± 0.08) x 10^{-14}	(2.9 ± 0.20) x 10^{-13}	(7.3 ± 0.60) x10^{-17}
Fish Lake	(4.2 ± 0.09) x 10^{-14}	(2.9 ± 0.06) x 10^{-13}	(3.2 ± 0.05) x10^{-16}
Lake Mendota	(3.7 ± 0.10) x 10^{-14}	(2.3 ± 0.02) x 10^{-13}	(4.7 ± 0.06) x10^{-17}
Lake Wingra	(4.0 ± 0.01) x 10^{-14}	(3.2 ± 0.05) x 10^{-13}	(6 ± 0.1) x10^{-17}
Big Muskellunge Lake	(1.5 ± 0.05) x 10^{-14}	(9 ± 1) x 10^{-14}	(6.8 ± 0.50) x 10^{-17}
Crystal Lake	(9.0 ± 0.10) x 10^{-15}	(2.6 ± 0.30) x 10^{-14}	(3.5 ± 0.60) x 10^{-17}
Sparkling Lake	(2.6 ± 0.13) x 10^{-14}	(7.9 ± 0.30) x 10^{-14}	(6.7 ± 0.70) x 10^{-17}
Trout Lake	(2.2 ± 0.03) x 10^{-14}	(7.7 ± 0.10) x 10^{-14}	(1.2 ± 0.10) x 10^{-16}

Table S9: Quantum yields (or quantum yield coefficients) for the sample waters. Error represents standard deviation in triplicate measurements.

Sample	f_{TMP} (M^{-1})	Φ_{1O2}	$\Phi_{\bullet OH}$
Trout Bog (D1)	16.3 ± 0.90	(4.6 ± 0.08) x 10^{-3}	(1.4± 0.006) x 10^{-4}
Crystal Bog (D2)	21.8 ± 2.2	(7.2± 0.08) x 10^{-3}	(1.1 ± 0.2) x 10^{-5}
Allequash Lake (M1)	42.6 ± 0.87	(1.8 ± 0.2) x 10^{-2}	(4.0 ± 0.6) x 10^{-5}
Lake Monona	130 ± 3.4	(3.83 ± 0.2) x 10^{-2}	(2.0 ± 0.2) x 10^{-5}
Fish Lake	103 ± 2.6	(3.7± 0.07) x 10^{-2}	(1.3 ± 0.02) x 10^{-4}
Lake Mendota	133 ± 4.5	(3.32 ± 0.04) x 10^{-2}	(2.2 ± 0.3) x 10^{-5}

Lake Wingra	79 ± 0.37	(2.21± 0.04) x 10^{-2}	(1.7 ± 0.03) x 10^{-5}
Big Muskellunge Lake	103 ± 4.4	(2.67 ± 0.4) x 10^{-2}	(7.3 ± 0.5) x 10^{-5}
Crystal Lake	91.4 ± 1.2	(2.76 ± 0.4) x 10^{-2}	(2.8 ± 0.5) x 10^{-5}
Sparkling Lake	92.8 ± 5.8	(1.70 ± 0.06) x 10^{-2}	(2.8 ± 0.3) x 10^{-5}
Trout Lake	55.5 ± 1.0	(1.97± 0.03) x 10^{-2}	(5.83 ± 0.5) x10^{-5}

Section S5: Quencher experiments

The sample waters were subset into a diverse DOM pool consisting of differing concentrations of PPRI (**Table S10**; **Figure S1**). This pool of DOM consists of dystrophic (D1-D2), mesotrophic (M1), eutrophic (E1-E2), and oligotrophic lakes (O1). D1 is characterized by relatively high concentrations of all three PPRI compared to the other sample waters. D2 is characterized by high concentrations of singlet oxygen with moderate to low concentrations of the other PPRI. M1 is characterized by moderate concentrations of all three PPRI. E1 is characterized by high triplet DOM and singlet oxygen and lower hydroxyl radicals. E2 is characterized by higher concentrations of all three PPRI. O1 is characterized by low concentrations of all three PPRI.

Table S10: Subset of waters used in the quenching experiments and the corresponding steady-state concentrations of PPRI in each sample water.

Sample	**Sample label**	**$[^3DOM]_{ss}$ (M)**	**$[^1O_2]_{ss}$ (M)**	**$[^{\bullet}OH]_{ss}$ (M)**
Trout Bog	D1	(3.89 ± 0.18) x 10^{-14}	(9.3 ± 0.2) x 10^{-13}	(1.8 ± 0.009) x 10^{-15}
Crystal Bog	D2	(3.04 ± 0.22) x 10^{-14}	(3.6 ± 0.04) x 10^{-13}	(9.5 ± 2) x 10^{-17}
Allequash Lake	M1	(3.14 ± 0.05) x 10^{-14}	(2.3 ± 0.2) x 10^{-13}	(1.7 ± 0.3) x 10^{-16}
Lake Monona	E1	(4.56 ± 0.08) x 10^{-14}	(2.9 ± 0.2) x 10^{-13}	(7.3 ± 0.6) x10^{-17}
Fish Lake	E2	(4.23 ± 0.09) x 10^{-14}	(2.9 ± 0.06) x 10^{-13}	(3.2 ± 0.05) x10^{-16}
Big Muskellunge Lake	O1	(1.49 ± 0.05) x 10^{-14}	(9.0 ± 1) x 10^{-14}	(6.8 ± 0.5) x 10^{-17}

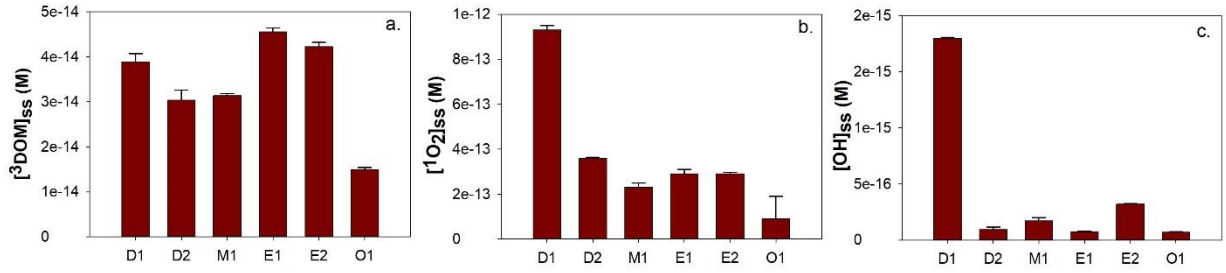

Figure S1: Comparison of PPRI steady-state concentrations between samples selected for quencher experiments and FT-ICR MS analysis. Steady-state concentrations of (a) ^{3}DOM (b) $^1O_2$, and (c) $^{\bullet}$OH. Error bars represent standard deviations between triplicate samples.

Optical properties pre- and post-photolysis. Samples containing no quenchers were used to investigate the general changes pre- and post-photolysis of each sample water. They were also used to compare the samples with no quenchers present to the samples with quenchers present to assess the responsibility of individual PPRI. **Table S11** as well as **Figures S2 (a-c)** provide summaries and visualizations of pre- and post-photolysis optical changes when no quenchers are present in a sample. E_2:E_3 was not added to this this table due to outliers present in multiple samples.

The changes in optical properties in samples with quenchers present was presented in **Table S12**. This table contains the fluorescence index and biological index. However, it does not contain $SUVA_{254}$ or E_2:E_3 because the absorbance was unable to be measured in the presence of the quenchers, which acted as an interferant in the measurements. The data was presented in terms of which PPRI is absent in the presence of the quencher the sample is treated with.

Table S11: Optical properties of sample waters without quenchers pre- and post-photolysis.

	FI		BIX		$SUVA_{254}$	
Sample	Pre	Post	Pre	Post	Pre	Post
Trout Bog (D1)	1.39	1.15	0.44	0.52	3.76	3.07
Crystal Bog (D2)	1.40	1.18	0.48	0.60	2.87	2.25
Allequash Lake (M1)	1.54	1.23	0.72	0.97	2.58	2.39
Lake Monona (E1)	1.65	1.27	0.96	1.26	1.67	1.53
Fish Lake (E2)	1.67	1.24	0.97	1.27	1.56	1.4
Big Muskellunge Lake (O1)	1.64	1.21	0.88	1.20	0.72	0.68

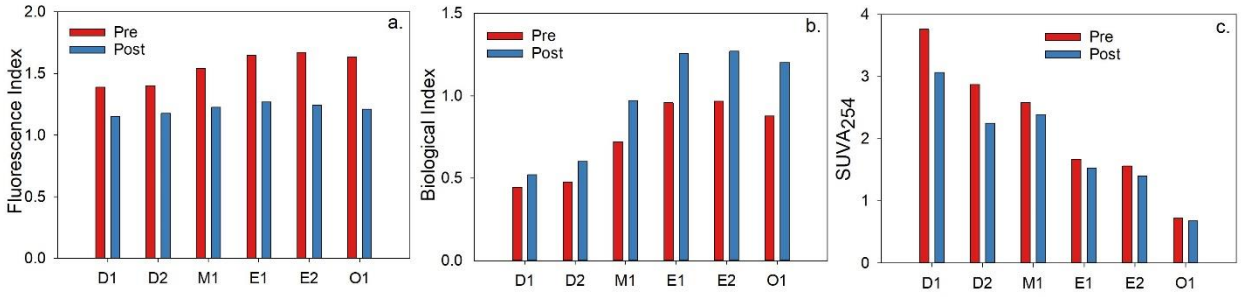

Figure S2: Changes in (a) fluorescence index, (b) biological index, and (c) $SUVA_{254}$ pre- and post-photolysis with no quenchers present (All PPRI present) in the sample waters.

Table S12: Optical properties of sample waters with quenchers pre- and post-photolysis.

		FI		BIX	
Sample	**Treatment**	**Pre**	**Post**	**Pre**	**Post**
Trout Bog (D1)	- $^{\bullet}OH$ (IPA)	1.38	1.13	0.45	0.56
	- $^{1}O_2$ (FFA)	1.36	1.03	0.46	0.67
	- ^{3}DOM (SA)	1.39	1.07	0.47	0.58
Crystal Bog (D2)	- $^{\bullet}OH$ (IPA)	1.42	1.15	0.46	0.61
	- $^{1}O_2$ (FFA)	1.38	1.06	0.54	0.79
	- ^{3}DOM (SA)	1.42	1.14	0.49	0.67
Allequash Lake (M1)	- $^{\bullet}OH$ (IPA)	1.57	1.23	0.74	1.02
	- $^{1}O_2$ (FFA)	1.45	1.30	0.86	1.15

	- ^{3}DOM (SA)	1.56	1.12	0.73	1.00
Lake Monona (E1)	- $^{\bullet}$OH (IPA)	1.63	1.22	0.99	1.33
	- $^1O_2$ (FFA)	1.51	1.10	1.10	1.55
	- ^{3}DOM (SA)	1.69	0.99	0.95	1.35
Fish Lake (E2)	- $^{\bullet}$OH (IPA)	1.68	1.27	0.98	1.25
	- $^1O_2$ (FFA)	1.57	1.20	1.06	1.45
	- ^{3}DOM (SA)	1.67	0.95	0.95	1.37
Big Muskellunge Lake (O1)	- $^{\bullet}$OH (IPA)	1.80	1.42	0.87	1.26
	- $^1O_2$ (FFA)	1.53	1.12	1.29	1.23
	- ^{3}DOM (SA)	1.48	1.02	0.85	1.12

Section S6: High-resolution mass spectrometry

Sample preparation methods. DOM was extracted from samples pre- and post-photolysis using solid phase extraction (SPE). Samples (250 mL) were acidified with hydrochloric acid (pH <2.0) and loaded onto BondElut PPL cartridges, which were activated using methanol (5 mL). The cartridges were rinsed with 0.1% HCl (1 mL), dried with air (5 minutes), and extracted with methanol (5 mL).

General molecular characteristics. Fourier transform-ion cyclotron mass spectrometry (FT-ICR MS) was performed on all the quenched and unquenched samples from the subset of sample waters. General characteristics such as weighted averages of H:C (H:C_w), O:C (O:C_w), and double bond equivalents per carbon (DBE/C), as well as number of formulas were calculated to investigate differences between quenched and unquenched samples to shed light on how certain PPRI are changing molecular DOM composition. These molecular characteristics are shown in **Table S13** and **Table S14**.

Table S13: General molecular characteristics including number of formulas and the number of CHO, CHON1, CHON2, and CHOS formulas. This included all sample treatments as well as analysis before and after 24-hour photolysis experiments.

		# total formulas		# CHO formulas		CHON1 formulas		CHON2 formulas		CHOS formulas	
Sample	**Treatment**	**Pre**	**Post**	**Pre**	**Post**	**Pre**	**Post**	**Pre**	**Post**	**Pre**	**Post**
Trout Bog (D1)	All PPRI	4407	4287	3353	3211	769	805	162	138	123	133
	- $^{\bullet}$OH (IPA)	3874	3808	3125	3038	579	608	68	96	102	66
	- $^{1}O_2$ (FFA)	4204	3975	3305	3056	712	725	65	54	122	140
	- ^{3}DOM (SA)	4514	4617	3514	3414	701	847	131	132	168	224
Crystal Bog (D2)	All PPRI	5047	5359	3176	3328	1439	1581	166	181	266	269
	- $^{\bullet}$OH (IPA)	5063	5225	3440	3292	1327	1498	140	150	156	285
	- $^{1}O_2$ (FFA)	4509	3797	3103	2741	1194	920	79	24	133	112
	- ^{3}DOM (SA)	5035	5249	3441	3409	1232	1431	178	197	184	212
Allequash Lake (M1)	All PPRI	4860	4937	3110	3094	1274	1342	213	221	263	280
	- $^{\bullet}$OH (IPA)	4778	4877	3063	3045	1285	1379	186	196	244	257
	- $^{1}O_2$ (FFA)	4188	3418	2785	2496	1174	792	73	36	156	94
	- ^{3}DOM (SA)	4548	4858	3013	3115	1055	1223	247	258	233	262
Lake Monona (E1)	All PPRI	5432	5301	2594	2470	1478	1499	589	569	771	763
	- $^{\bullet}$OH (IPA)	5458	5218	2583	2515	1536	1418	516	508	823	777
	- $^{1}O_2$ (FFA)	4708	4113	2578	2615	1432	1031	167	99	531	368
	- ^{3}DOM (SA)	5192	5622	2485	2616	1377	1514	573	650	757	842
Fish Lake (E2)	All PPRI	5490	5469	2639	2548	1669	1708	740	752	442	461
	- $^{\bullet}$OH (IPA)	5720	5387	2763	2626	1722	1663	801	687	434	411
	- $^{1}O_2$ (FFA)	4779	3978	2705	2592	1618	1156	211	118	245	112
	- ^{3}DOM (SA)	5479	5482	2647	2650	1593	1592	798	790	441	450
Big Muskellunge Lake (O1)	All PPRI	5658	5196	2837	2611	1907	1598	406	472	508	515
	- $^{\bullet}$OH (IPA)	5375	5084	2736	2628	1611	1528	484	426	544	502
	- $^{1}O_2$ (FFA)	4202	3643	2389	2414	1400	902	124	59	289	268
	- ^{3}DOM (SA)	4831	4872	2531	2569	1363	1354	440	471	497	478

Table S14: General molecular characteristics including H:C_w, O:C_w, and DBE/C_w for all sample treatments as well as analysis before and after 24-hr photolysis experiments.

		H:C_w		O:C_w		DBE/C	
Sample	**Treatment**	**Pre**	**Post**	**Pre**	**Post**	**Pre**	**Post**
Trout Bog (D1)	All PPRI	1.09	1.05	0.53	0.55	0.51	0.53
	- $^{\bullet}$OH (IPA)	1.20	1.21	0.47	0.45	0.46	0.45

	- $^1O_2$ (FFA)	1.10	1.07	0.51	0.52	0.51	0.52
	- ^{3}DOM (SA)	1.12	1.09	0.51	0.52	0.49	0.51
Crystal Bog (D2)	All PPRI	1.14	1.14	0.51	0.52	0.49	0.49
	- $^{\bullet}$OH (IPA)	1.14	1.16	0.51	0.50	0.48	0.48
	- $^1O_2$ (FFA)	1.14	1.11	0.49	0.52	0.48	0.50
	- ^{3}DOM (SA)	1.11	1.11	0.52	0.52	0.50	0.50
Allequash Lake (M1)	All PPRI	1.19	1.20	0.50	0.51	0.46	0.46
	- $^{\bullet}$OH (IPA)	1.19	1.20	0.50	0.50	0.47	0.46
	- $^1O_2$ (FFA)	1.16	1.11	0.49	0.53	0.48	0.50
	- ^{3}DOM (SA)	1.20	1.18	0.50	0.51	0.46	0.47
Lake Monona (E1)	All PPRI	1.32	1.30	0.46	0.48	0.41	0.42
	- $^{\bullet}$OH (IPA)	1.30	1.33	0.47	0.45	0.42	0.40
	- $^1O_2$ (FFA)	1.25	1.16	0.47	0.52	0.44	0.48
	- ^{3}DOM (SA)	1.29	1.28	0.47	0.47	0.42	0.43
Fish Lake (E2)	All PPRI	1.27	1.27	0.51	0.51	0.43	0.44
	- $^{\bullet}$OH (IPA)	1.26	1.26	0.51	0.52	0.44	0.44
	- $^1O_2$ (FFA)	1.23	1.16	0.49	0.53	0.45	0.48
	- ^{3}DOM (SA)	1.26	1.25	0.51	0.52	0.44	0.45
Big Muskellunge Lake (O1)	All PPRI	1.33	1.30	0.50	0.50	0.40	0.42
	- $^{\bullet}$OH (IPA)	1.30	1.29	0.49	0.49	0.41	0.42
	- $^1O_2$ (FFA)	1.25	1.13	0.49	0.53	0.44	0.49
	- ^{3}DOM (SA)	1.29	1.28	0.49	0.49	0.42	0.42

Formula intensity change. Relative formula intensity before and after photolysis was analyzed to investigate how DOM molecular composition changed throughout photolysis with different quenchers present. This analysis was done on formulas that changed in intensity but were present before and after photolysis. The intensity changes of a sample water with a quencher that went through photolysis was compared to a dark control with the same quencher present. Relative intensity changes of formulas present before (t0) and after photolysis (t24) were separated into two groups: formulas that increased in relative intensity by ≥10% and formulas that decreased in relative intensity by ≥10% after photolysis. The H:C and O:C ratios of each of formulas in these groups were calculated and plotted with each other. **Figure S3** shows the increasing and decreasing

relative formula intensity van Krevelen diagrams for all treatments and sample waters used in the quencher experiments.

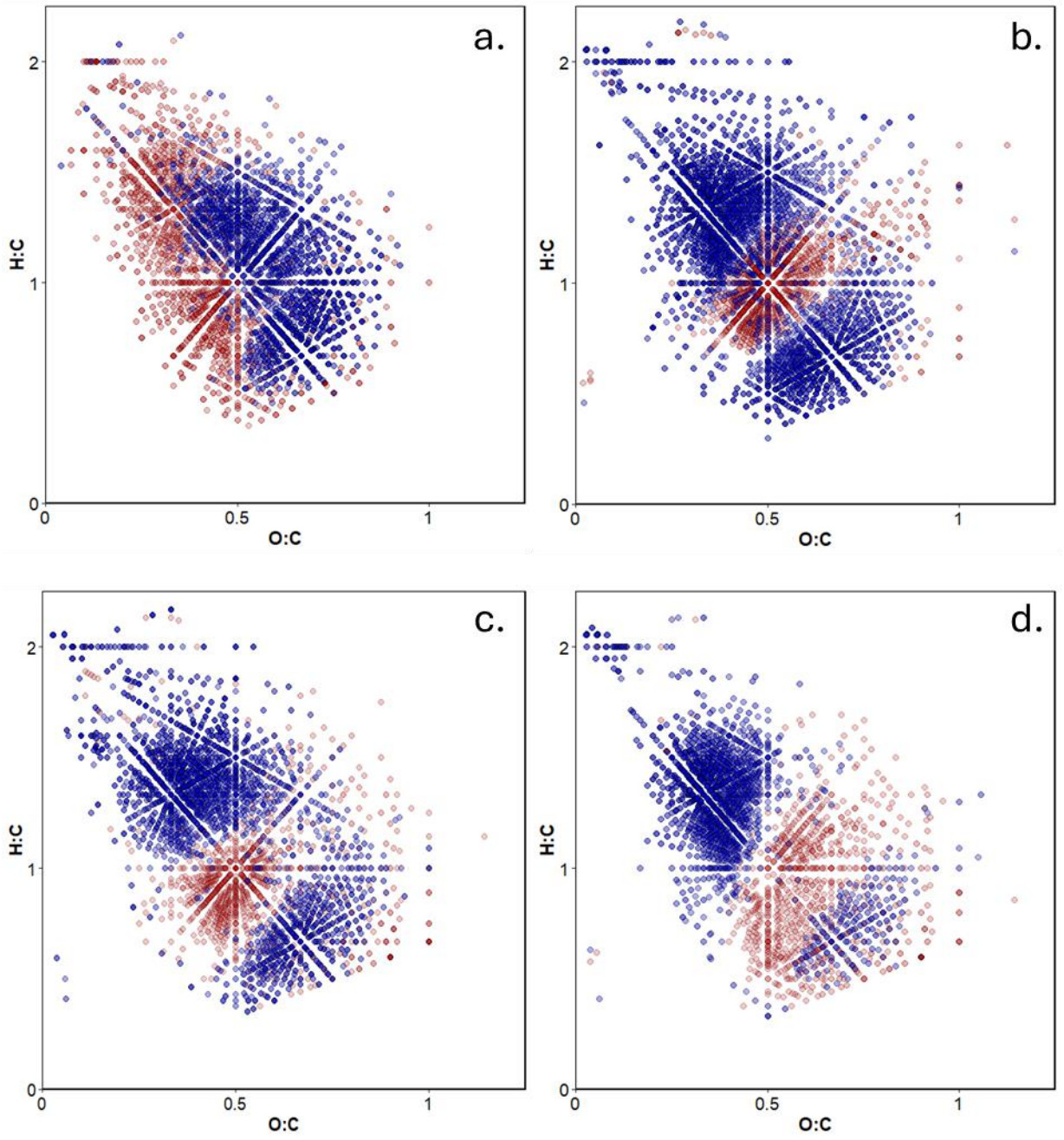

Figure S3: Relative formula intensity increase/decrease van Krevelen diagrams, with blue representing formula intensity decreases ≥10% and red representing formula intensity increases ≥10%. Each individual graph represents a treatment from Trout Bog (D1) including (a) -$^{\bullet}$OH (IPA), (b) -$^{1}O_2$ (FFA), (c) -^{3}DOM (SA), and (d) All PPRI.

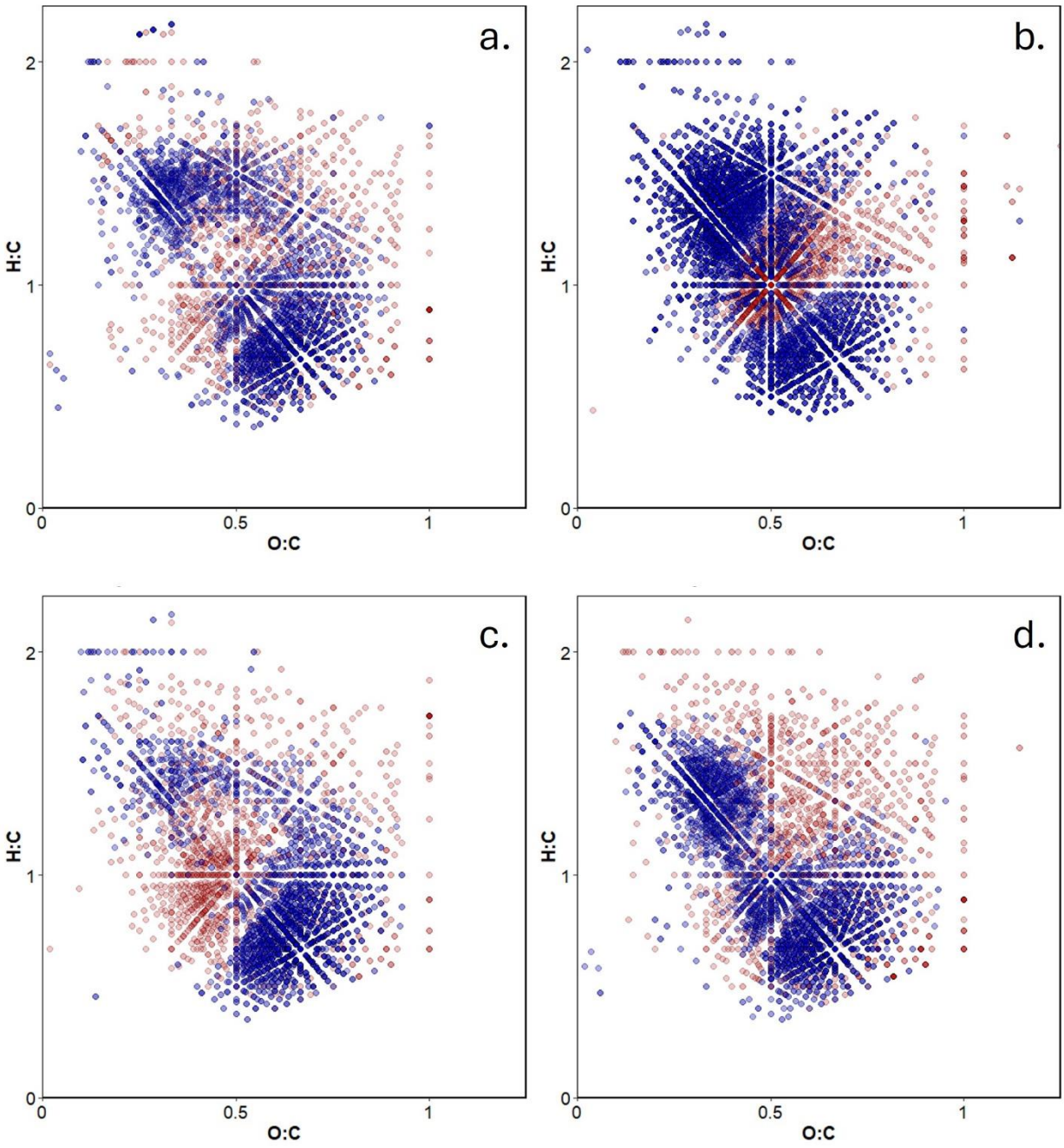

Figure S4: Relative formula intensity increase/decrease van Krevelen diagrams, with blue representing formula intensity decreases ≥10% and red representing formula intensity increases ≥10%. Each individual graph represents a treatment from Crystal Bog (D2) including (a) -•OH (IPA), (b) -$^{1}O_{2}$ (FFA), (c) -^{3}DOM (SA), and (d) All PPRI.

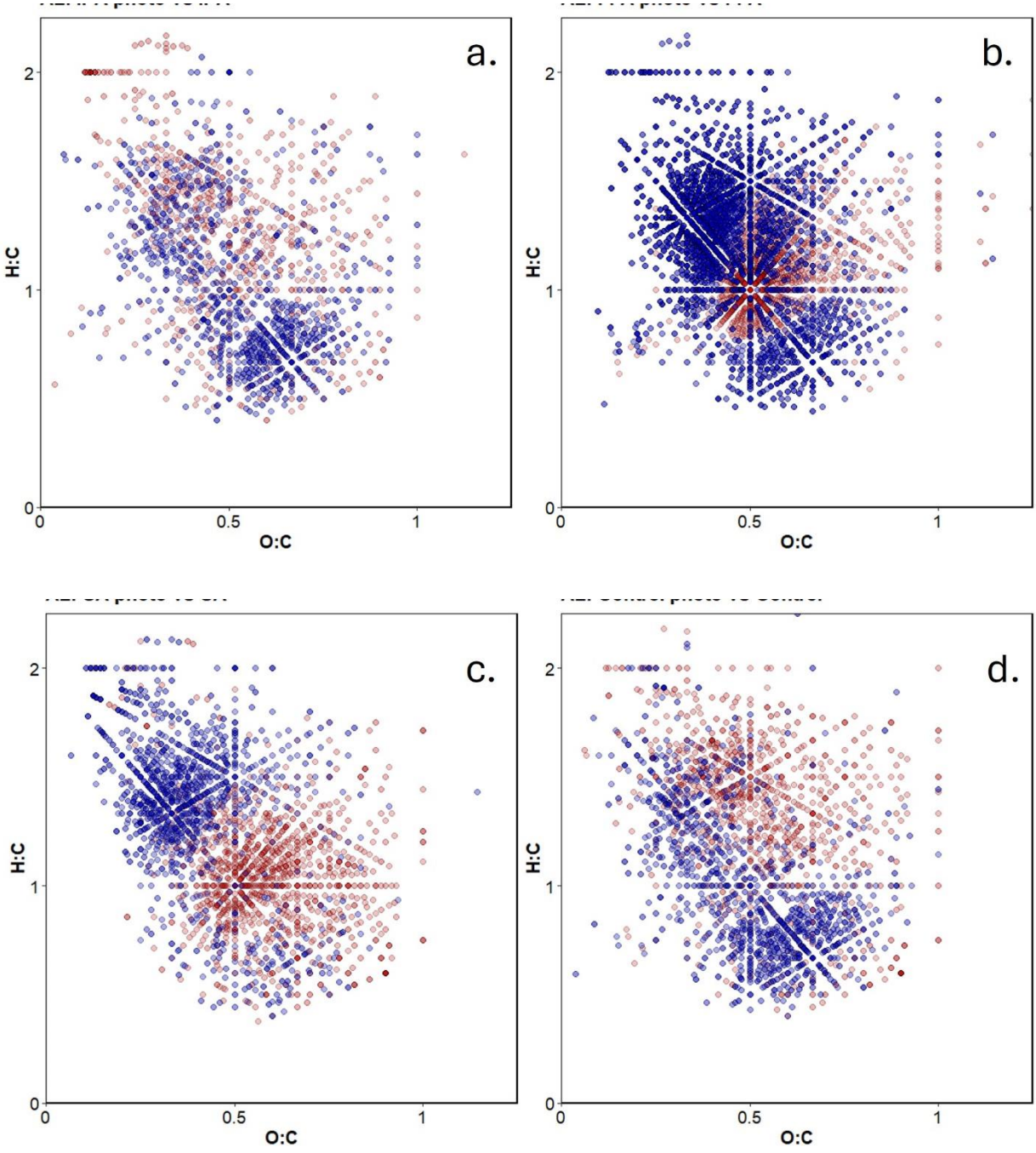

Figure S5: Relative formula intensity increase/decrease van Krevelen diagrams, with blue representing formula intensity decreases ≥10% and red representing formula intensity increases ≥10%. Each individual graph represents a treatment from Allequash Lake (M1) including (a) -•OH (IPA), (b) -$^{1}O_{2}$ (FFA), (c) -^{3}DOM (SA), and (d) All PPRI.

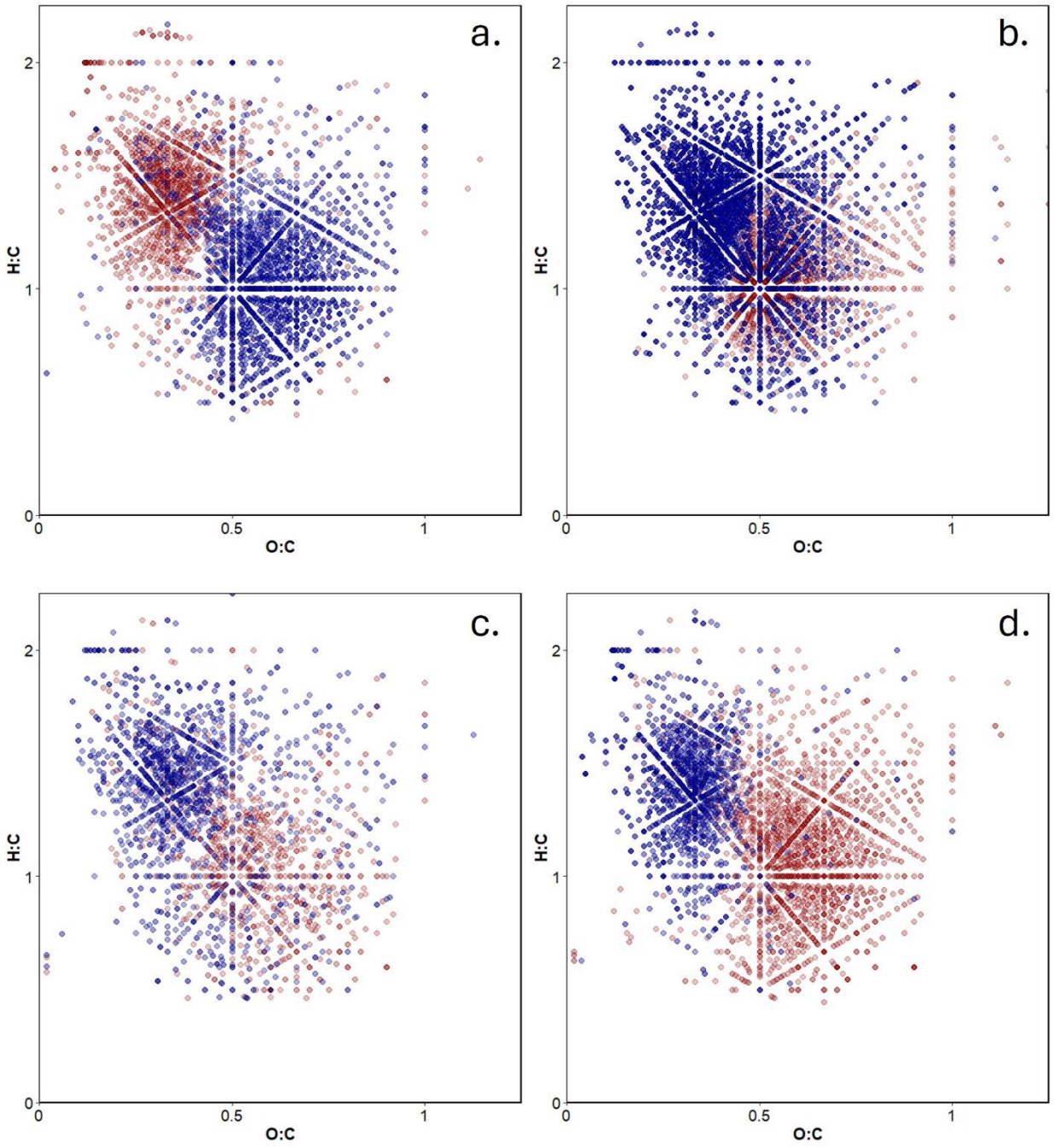

Figure S6: Relative formula intensity increase/decrease van Krevelen diagrams, with blue representing formula intensity decreases ≥10% and red representing formula intensity increases ≥10%. Each individual graph represents a treatment from Lake Monona (E1) including (a) -•OH (IPA), (b) -$^{1}O_2$ (FFA), (c) -^{3}DOM (SA), and (d) All PPRI.

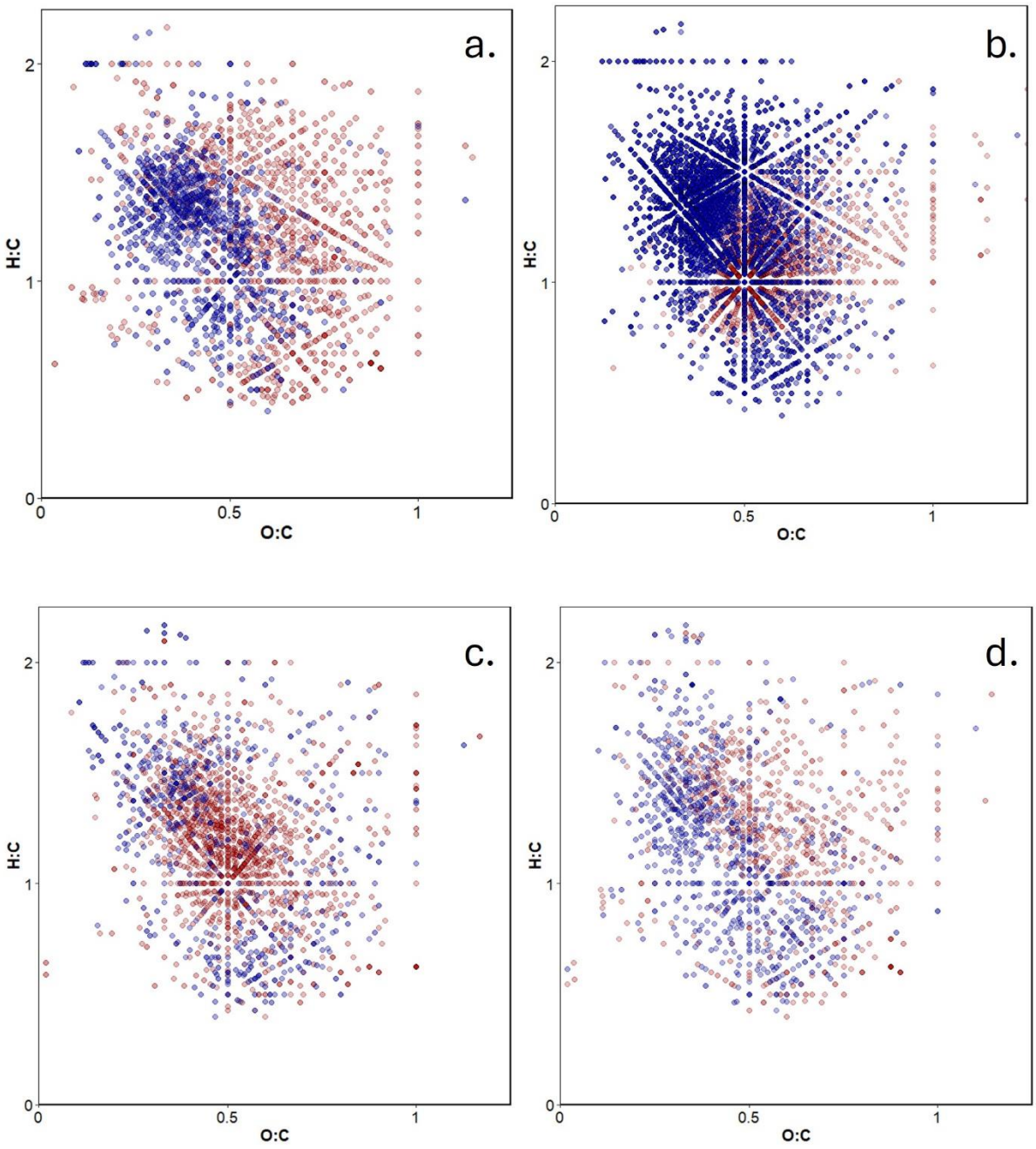

Figure S7: Relative formula intensity increase/decrease van Krevelen diagrams, with blue representing formula intensity decreases ≥10% and red representing formula intensity increases ≥10%. Each individual graph represents a treatment from Fish Lake (E2) including (a) -•OH (IPA), (b) -$^1O_2$ (FFA), (c) -^{3}DOM (SA), and (d) All PPRI.

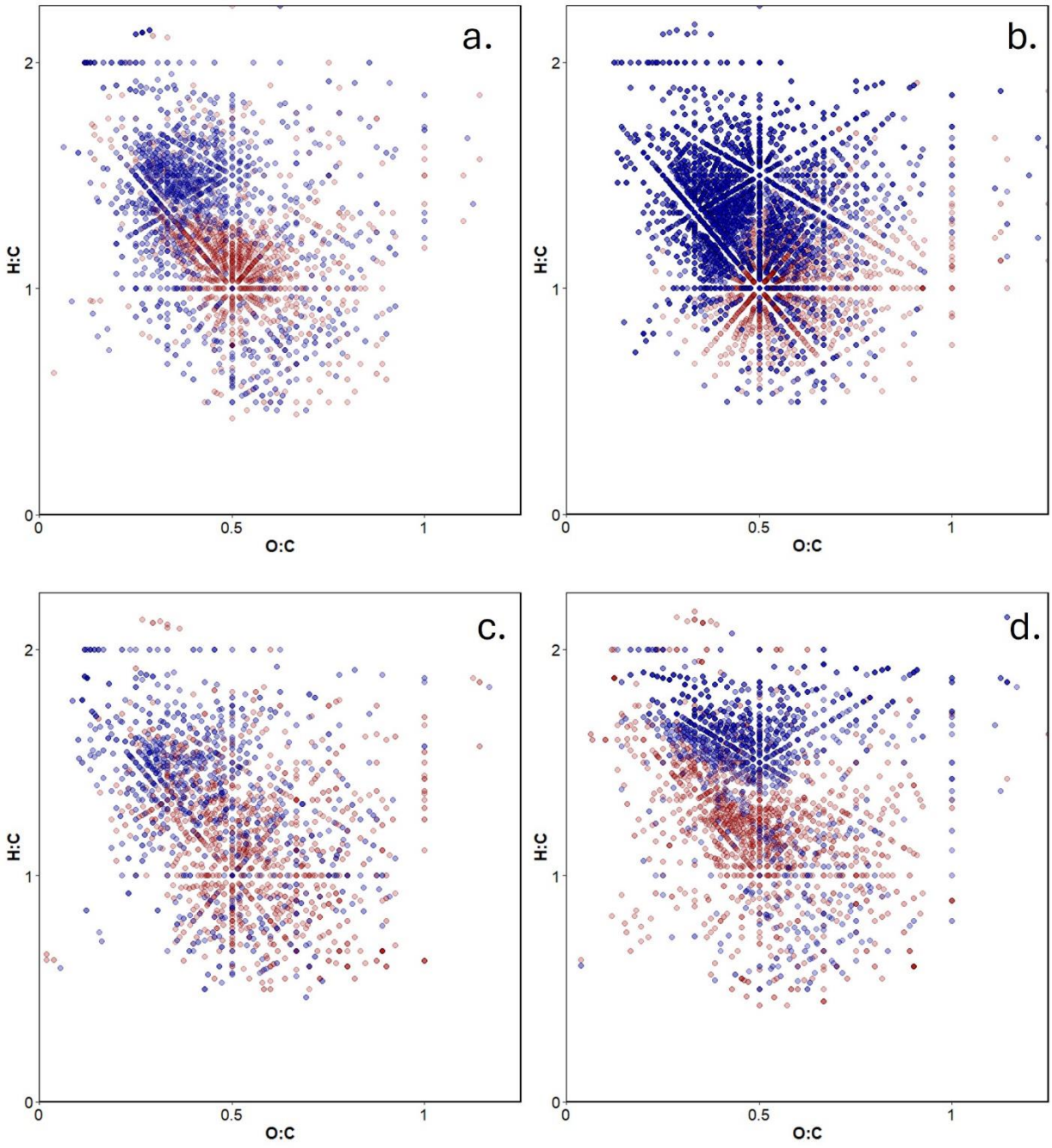

Figure S8: Relative formula intensity increase/decrease van Krevelen diagrams, with blue representing formula intensity decreases ≥10% and red representing formula intensity increases ≥10%. Each individual graph represents a treatment from Big Muskellunge Lake (O1) including (a) -$^{\bullet}$OH (IPA), (b) -$^{1}O_2$ (FFA), (c) -^{3}DOM (SA), and (d) All PPRI.

O addition and CO_2 loss formulas. DOM molecular composition changes were analyzed for partial and complete photooxidation. To do this, formulas showing evidence of oxygen addition and carbon dioxide loss were analyzed. Oxygen addition pathways (+1O, +2O, +1O/+2O) were analyzed by constructing mass lists based on the formulas in each dark control for each treatment in each sample water. Then, each mass list was searched for predicted unique photoproducts in the irradiated samples that corresponded to their respective dark controls. This allows the addition of one, two, or one/two oxygen atoms to be quantified in the formula matching of the irradiated sample. One/two oxygen addition was quantified if the formation of the product can be attributed to either the addition of one oxygen or two oxygen pathways. This can be used to give insight into the partial photooxidation of the DOM in the presence of different PPRI/quenchers.

Carbon dioxide loss was quantified through the generation of a mass list based on formulas in the dark controls for each treatment in each sample water. Then this mass list was used to search for predicted carbon dioxide loss products in the irradiated samples. This can be used to give insight into complete photooxidation of the DOM in the presence of different PPRI/quenchers. The number of oxygen addition and carbon dioxide loss formulas were presented in **Table S15 and Figure S9**. van Krevelen diagrams showcasing how DOM composition effects oxygen addition and carbon dioxide loss were presented in **Figure S10-S15**.

Table S15: Number of oxygen addition and carbon dioxide loss formulas in each sample water and treatment.

Sample	Treatment	# 1O addition	# 2O addition	# 1O/2O addition	# of total O addition	# CO2 loss

Trout Bog (D1)	- $^{\bullet}OH$	66	51	92	209	299
	- $^{1}O_2$	93	101	345	539	207
	- ^{3}DOM	52	75	114	241	139
	All PPRI	63	59	177	299	130
Crystal Bog (D2)	- $^{\bullet}OH$	57	44	127	228	136
	- $^{1}O_2$	29	93	186	308	37
	- ^{3}DOM	63	55	111	259	181
	All PPRI	83	105	234	422	151
Allequash Lake (M1)	- $^{\bullet}OH$	85	66	129	280	154
	- $^{1}O_2$	34	81	181	296	36
	- ^{3}DOM	105	115	169	389	161
	All PPRI	91	76	157	324	150
Lake Monona (E1)	- $^{\bullet}OH$	57	48	69	174	235
	- $^{1}O_2$	39	108	226	373	662
	- ^{3}DOM	98	95	194	387	197
	All PPRI	64	83	196	343	480
Fish Lake (E2)	- $^{\bullet}OH$	67	63	159	289	105
	- $^{1}O_2$	41	108	203	352	41
	- ^{3}DOM	96	83	142	321	161
	All PPRI	75	75	145	295	143
Big Muskellunge Lake (O1)	- $^{\bullet}OH$	41	52	87	180	106
	- $^{1}O_2$	36	88	180	304	51
	- ^{3}DOM	81	72	158	311	158

	All PPRI	46	48	88	182	216

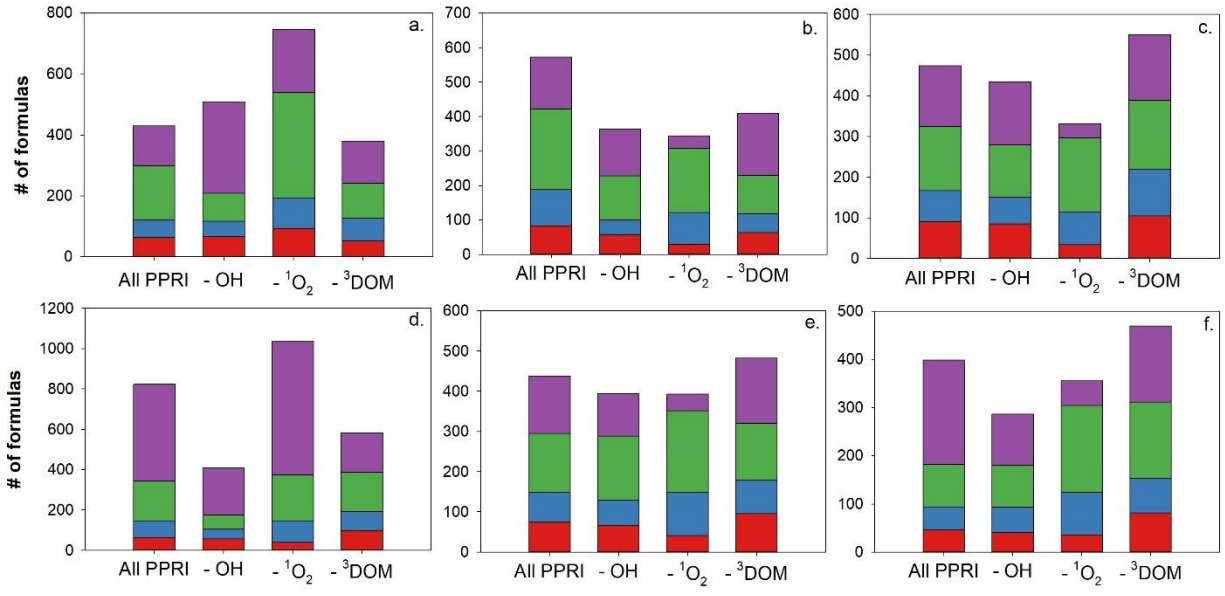

Figure S9: Bar graphs demonstrating the number of oxygen additions and carbon dioxide loss in each sample water and treatment. Red represents one oxygen addition, blue represents two oxygen additions, green represents either one or two oxygen additions, and purple represents carbon dioxide loss. Each individual graph represents a sample water including (a) D1, (b) D2, (c) M1, (d) E1, (e) E2, and (f) O1.

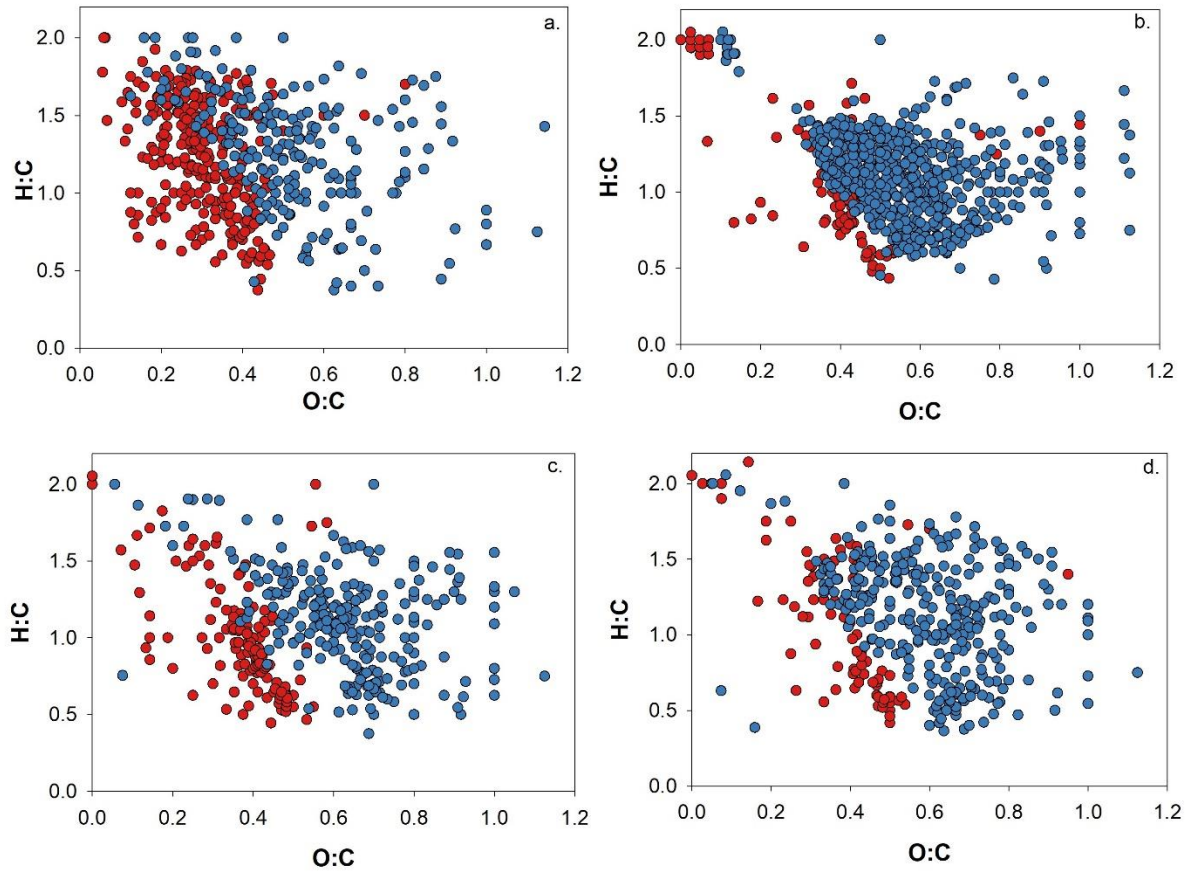

Figure S10: van Krevelen diagrams demonstrating the DOM compositional differences in oxygen addition and carbon dioxide loss in each sample water and treatment. Red represents carbon dioxide loss formulas and blue represents total oxygen addition formulas. Each individual graph represents a treatment from Trout Bog (D1) including (a) -$^{\bullet}$OH (IPA), (b) -$^{1}O_2$ (FFA), (c) -^{3}DOM (SA), and (d) All PPRI.

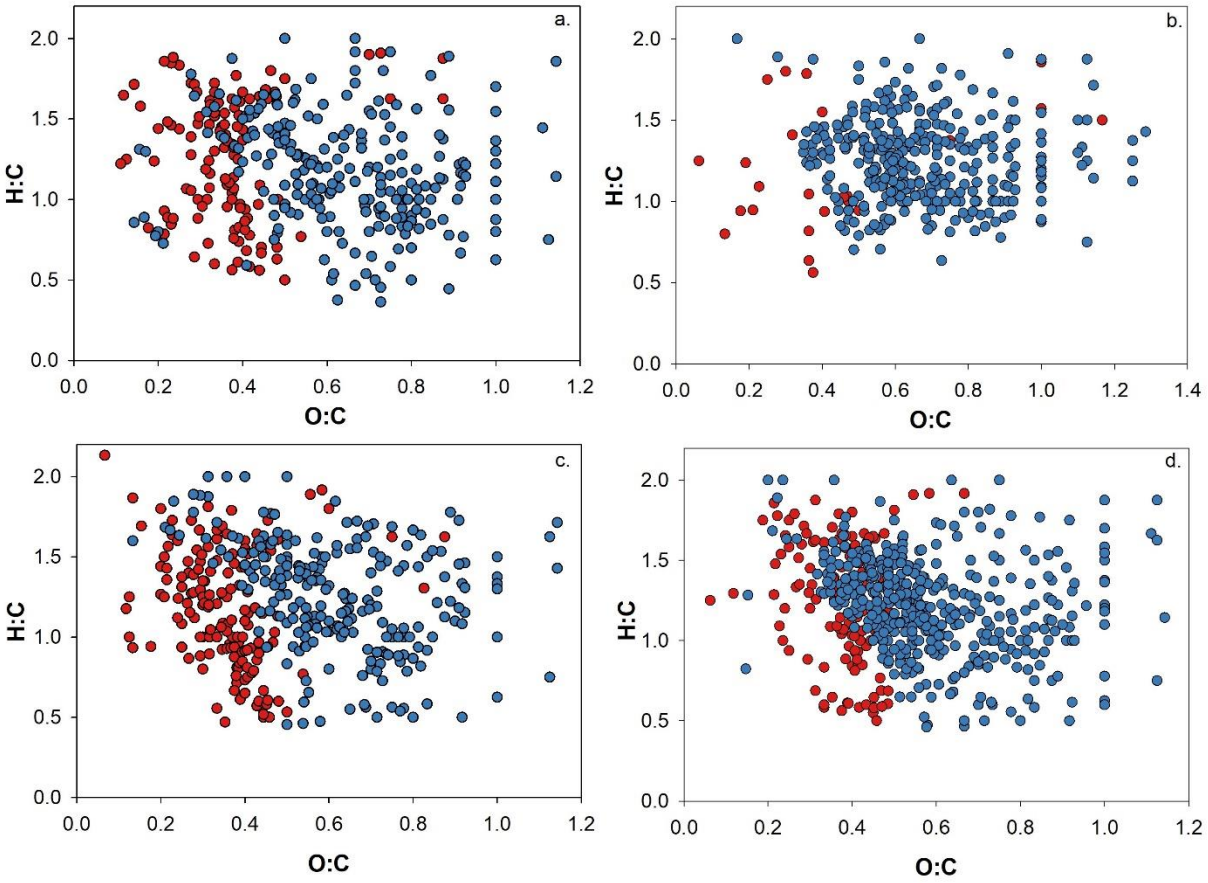

Figure S11: van Krevelen diagrams demonstrating the DOM compositional differences in oxygen addition and carbon dioxide loss in each sample water and treatment. Red represents carbon dioxide loss formulas and blue represents total oxygen addition formulas. Each individual graph represents a treatment from Crystal Bog (D2) including (a) -$^{\bullet}$OH (IPA), (b) -$^{1}O_2$ (FFA), (c) -^{3}DOM (SA), and (d) All PPRI.

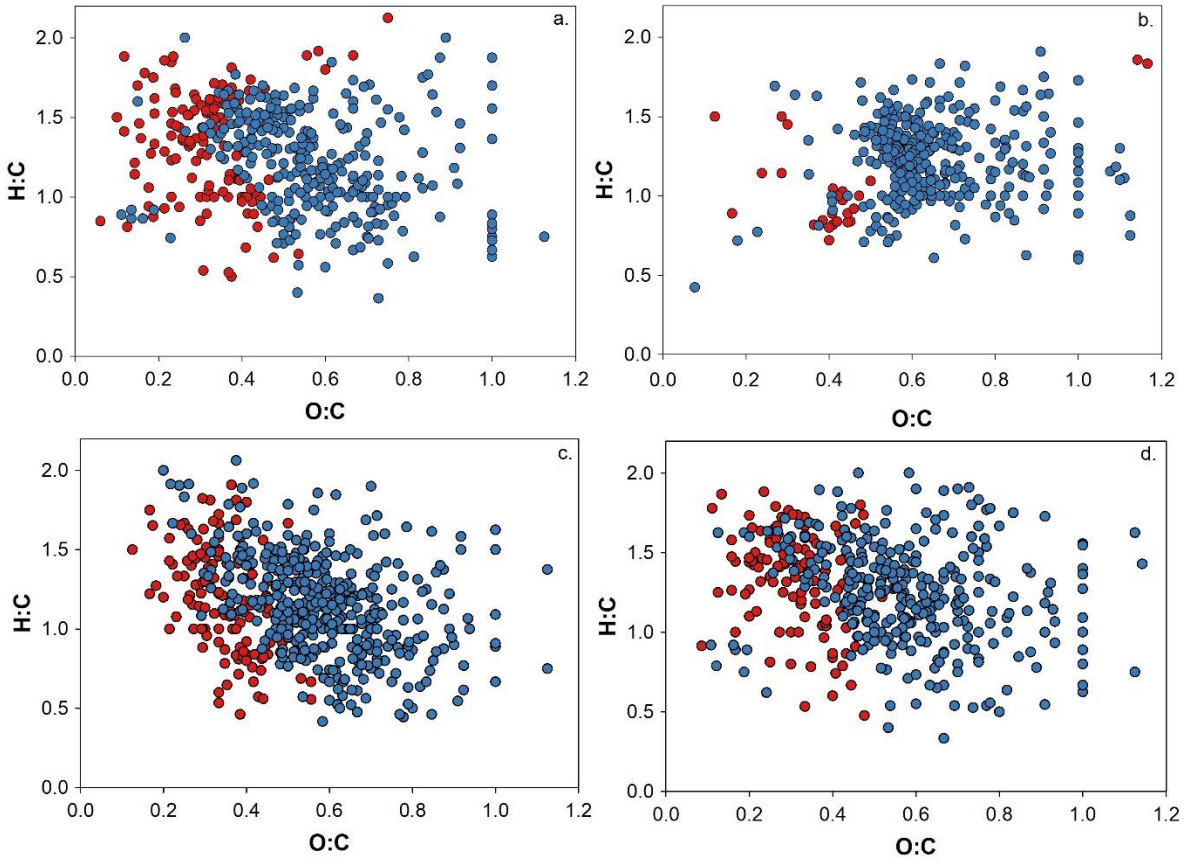

Figure S12: van Krevelen diagrams demonstrating the DOM compositional differences in oxygen addition and carbon dioxide loss in each sample water and treatment. Red represents carbon dioxide loss formulas and blue represents total oxygen addition formulas. Each individual graph represents a treatment from Allequash Lake (M1) including (a) -$^{\bullet}$OH (IPA), (b) -$^{1}O_2$ (FFA), (c) -^{3}DOM (SA), and (d) All PPRI.

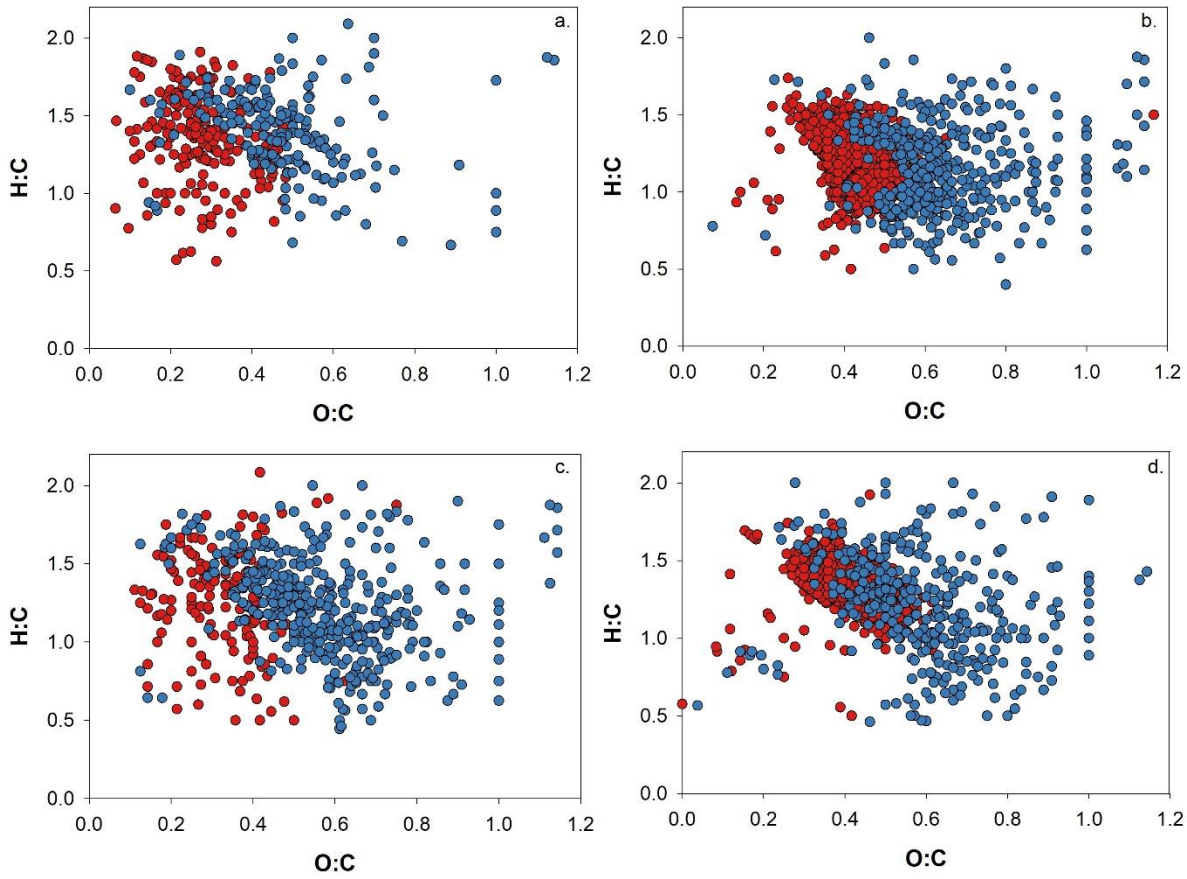

Figure S13: van Krevelen diagrams demonstrating the DOM compositional differences in oxygen addition and carbon dioxide loss in each sample water and treatment. Red represents carbon dioxide loss formulas and blue represents total oxygen addition formulas. Each individual graph represents a treatment from Lake Monona (E1) including (a) -$^{\bullet}$OH (IPA), (b) -$^{1}O_2$ (FFA), (c) -^{3}DOM (SA), and (d) All PPRI.

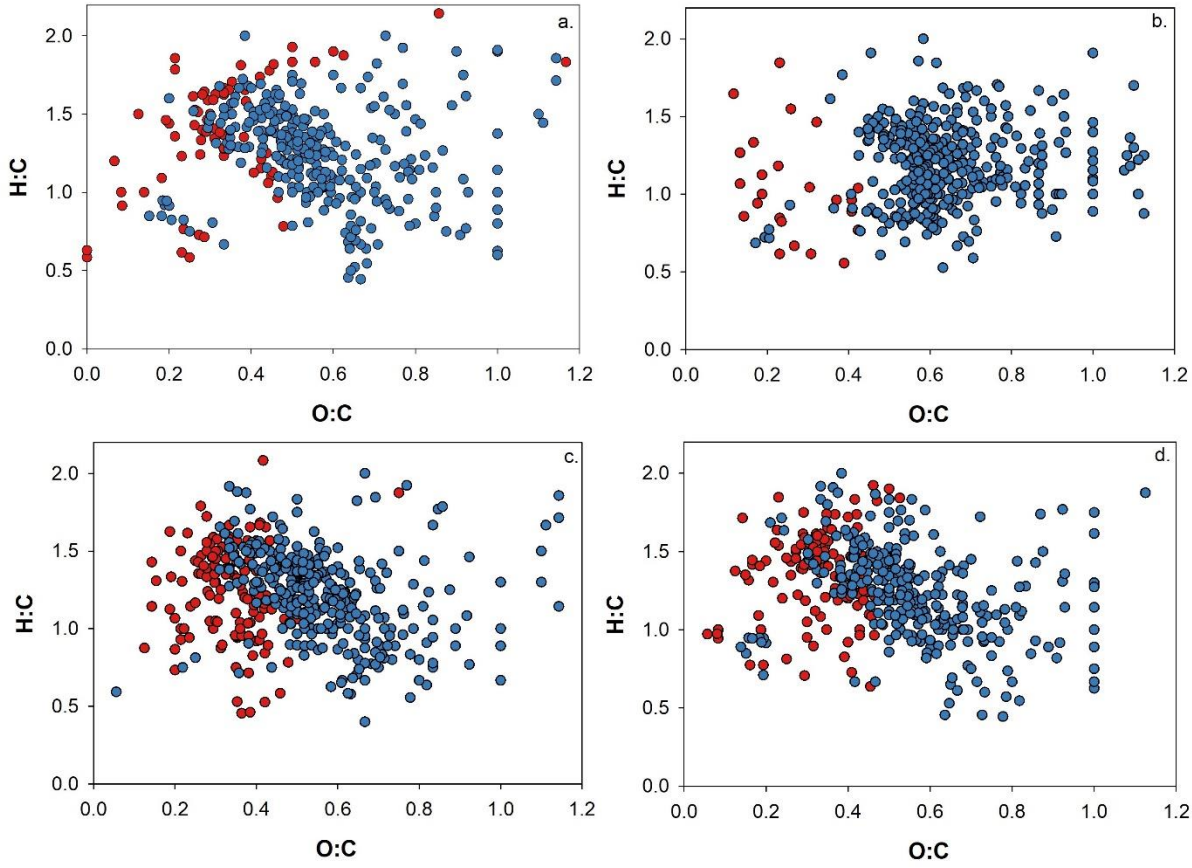

Figure S14: van Krevelen diagrams demonstrating the DOM compositional differences in oxygen addition and carbon dioxide loss in each sample water and treatment. Red represents carbon dioxide loss formulas and blue represents total oxygen addition formulas. Each individual graph represents a treatment from Fish Lake (E2) including (a) -$^{\bullet}$OH (IPA), (b) -$^{1}O_2$ (FFA), (c) -^{3}DOM (SA), and (d) All PPRI.

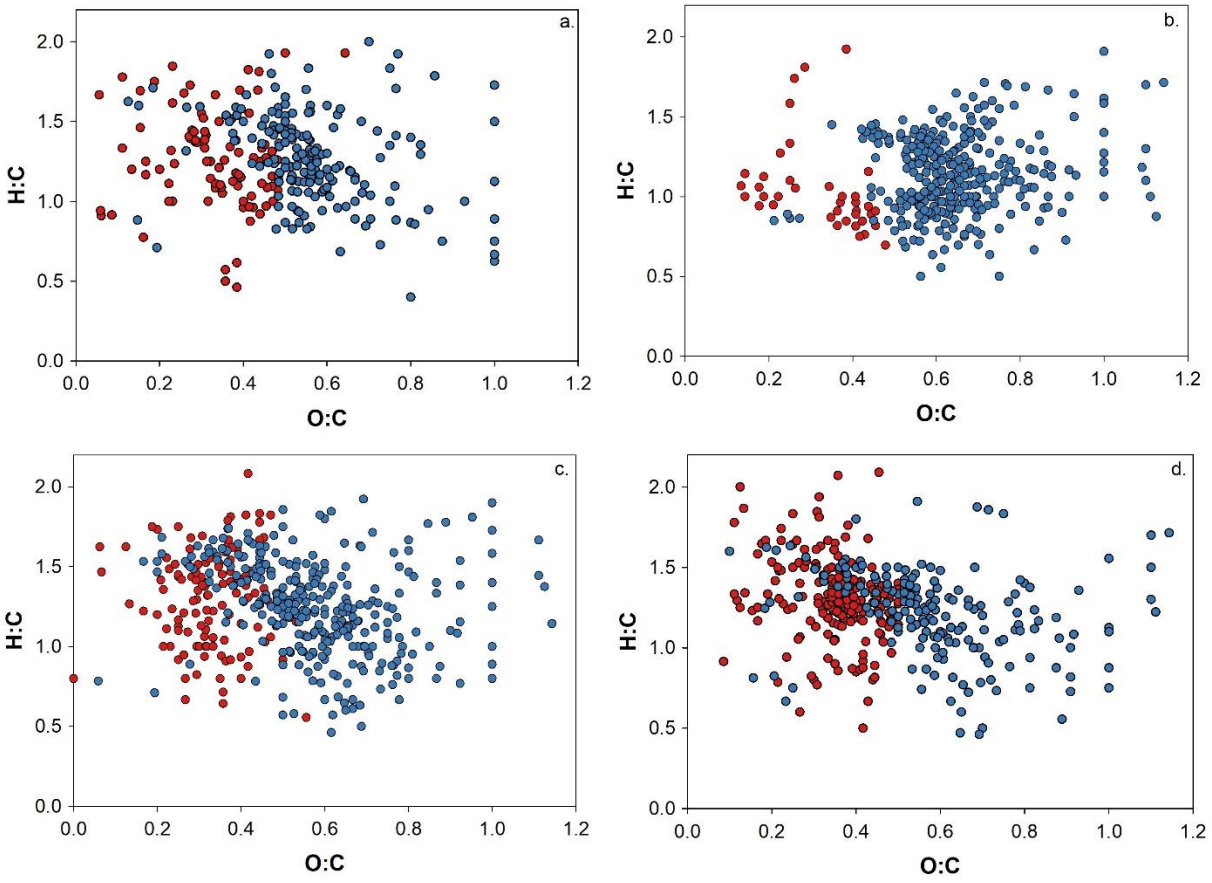

Figure S15: van Krevelen diagrams demonstrating the DOM compositional differences in oxygen addition and carbon dioxide loss in each sample water and treatment. Red represents carbon dioxide loss formulas and blue represents total oxygen addition formulas. Each individual graph represents a treatment from Big Muskellunge Lake (O1) including (a) -$^{\bullet}$OH (IPA), (b) -$^{1}O_2$ (FFA), (c) -^{3}DOM (SA), and (d) All PPRI.

Section S7: References

(1) https://lter.limnology.wisc.edu/. *North Temperate Lakes US Long-Term Ecological Research Network*.

(2) Huguet, A.; Vacher, L.; Relexans, S.; Saubusse, S.; Froidefond, J. M.; Parlanti, E. Properties of Fluorescent Dissolved Organic Matter in the Gironde Estuary. *Organic Geochemistry* **2009**, *40* (6), 706–719. https://doi.org/10.1016/j.orggeochem.2009.03.002.

(3) McKnight, D. M.; Boyer, E. W.; Westerhoff, P. K.; Doran, P. T.; Kulbe, T.; Andersen, D. T. Spectrofluorometric Characterization of Dissolved Organic Matter for Indication of Precursor Organic Material and Aromaticity. *Limnology Oceanography* **2001**, *46* (1), 38–48. https://doi.org/10.4319/lo.2001.46.1.0038.

(4) Helms, J. R.; Stubbins, A.; Ritchie, J. D.; Minor, E. C.; Kieber, D. J.; Mopper, K. Absorption Spectral Slopes and Slope Ratios as Indicators of Molecular Weight, Source, and Photobleaching of Chromophoric Dissolved Organic Matter. *Limnology Oceanography* **2008**, *53* (3), 955–969. https://doi.org/10.4319/lo.2008.53.3.0955.

(5) Weishaar, J. L.; Aiken, G. R.; Bergamaschi, B. A.; Fram, M. S.; Fujii, R.; Mopper, K. Evaluation of Specific Ultraviolet Absorbance as an Indicator of the Chemical Composition and Reactivity of Dissolved Organic Carbon. *Environmental Science Technology* **2003**, *37* (20), 4702–4708. https://doi.org/10.1021/es030360x.

(6) Maizel, A. C.; Remucal, C. K. The Effect of Probe Choice and Solution Conditions on the Apparent Photoreactivity of Dissolved Organic Matter. *Environmental Science Process Impacts* **2017**, *19* (8), 1040–1050. https://doi.org/10.1039/c7em00235a.

(7) Page, S. E.; Arnold, W. A.; McNeill, K. Terephthalate as a Probe for Photochemically Generated Hydroxyl Radical. *Journal of Environmental Monitoring* **2010**, *12* (9), 1658–1665. https://doi.org/10.1039/c0em00160k.

(8) Laszakovits, J. R.; Berg, S. M.; Anderson, B. G.; O'Brien, J. E.; Wammer, K. H.; Sharpless, C. M. P-Nitroanisole/Pyridine and p-Nitroacetophenone/Pyridine Actinometers Revisited: Quantum Yield in Comparison to Ferrioxalate. *Environmental Science Technology Letters* **2017**, *4* (1), 11–14. https://doi.org/10.1021/acs.estlett.6b00422.

(9) Maizel, A. C.; Remucal, C. K. Molecular Composition and Photochemical Reactivity of Size-Fractionated Dissolved Organic Matter. *Environmental Science Technology* **2017**, *51* (4), 2113–2123. https://doi.org/10.1021/acs.est.6b05140.

(10) Appiani, E.; Ossola, R.; Latch, D. E.; Erickson, P. R.; McNeill, K. Aqueous Singlet Oxygen Reaction Kinetics of Furfuryl Alcohol: Effect of Temperature, PH, and Salt Content.

Environmental Science Process Impacts **2017**, *19* (4), 507–516. https://doi.org/10.1039/c6em00646a.

(11) Maizel, A. C.; Li, J.; Remucal, C. K. Relationships between Dissolved Organic Matter Composition and Photochemistry in Lakes of Diverse Trophic Status. *Environmental Science Technology* **2017**, *51* (17), 9624–9632. https://doi.org/10.1021/acs.est.7b01270.

(12) Canonica, S.; Jans, U.; Stemmler, K.; Hoigné, J. Transformation Kinetics of Phenols in Water: Photosensitization by Dissolved Natural Organic Material and Aromatic Ketones; 1995; Vol. 29. https://pubs.acs.org/sharingguidelines.

(13) Jasper, J. T.; Sedlak, D. L. Phototransformation of Wastewater-Derived Trace Organic Contaminants in Open-Water Unit Process Treatment Wetlands. *Environmental Science Technology* **2013**, *47* (19), 10781–10790. https://doi.org/10.1021/es304334w.

(14) Westerhoff, P.; Mezyk, S. P.; Cooper, W. J.; Minakata, D. Electron Pulse Radiolysis Determination of Hydroxyl Radical Rate Constants with Suwannee River Fulvic Acid and Other Dissolved Organic Matter Isolates. *Environmental Science Technology* **2007**, *41* (13), 4640–4646. https://doi.org/10.1021/es062529n.

(15) Berg, S. M.; Wammer, K. H.; Remucal, C. K. Dissolved Organic Matter Photoreactivity Is Determined by Its Optical Properties, Redox Activity, and Molecular Composition. *Environmental Science Technology* **2023**, *57* (16), 6703–6711. https://doi.org/10.1021/acs.est.3c01157.